Bone hydration: how to can evaluate it, what can it tell us, and is it an effective therapeutic target?

Rachel K. Surowiec[1,2], Matthew R. Allen[1,2,3] and Joseph M. Wallace[2]

[1]Department of Anatomy, Cell Biology & Physiology, Indiana University School of Medicine, Indianapolis IN, United States

[2]Department of Biomedical Engineering, Indiana University Purdue University of Indianapolis, Indianapolis, IN, United States.

[3]Roudebush Veterans Administration Medical Center, Indianapolis, IN, United States.

Disclosures:

All authors declare that they have no conflicts of interest.

Send Correspondence to:

Rachel K. Surowiec, PhD

rksurowi@iu.edu

350 N. Blackford St. EL221

Indianapolis, Indiana 46202

United States

Abstract

Water constitutes roughly a quarter of the cortical bone by volume yet can greatly influence mechanical properties and tissue quality. There is a growing appreciation for how water can dynamically change due to age, disease, and treatment. A key emerging area related to bone mechanical and tissue properties lies in differentiating the role of water in its four different compartments, including free/pore water, water loosely bound at the collagen/mineral interfaces, water tightly bound within collagen triple helices, and structural water within the mineral. This review summarizes our current knowledge of bone water across the four functional compartments and discuss how alterations in each compartment relate to mechanical changes. It provides an overview on the advent of- and improvements to- imaging and spectroscopic techniques able to probe nano-and molecular scales of bone water. These technical advances have led to an emerging understanding of how bone water changes in various conditions, of which aging, chronic kidney disease, diabetes, osteoporosis, and osteogenesis imperfecta are reviewed. Finally, it summarizes work focused on therapeutically targeting water to improve mechanical properties.

Key Words: Bone water, skeletal imaging, bound water, free water, structural water, mechanical properties, material quality

1. Introduction

Bone is a highly heterogeneous composite biomaterial comprised of mineral, collagen, and water. These bone building blocks maintain a complex and dynamic structural hierarchy across discrete length scales that span organ-level, micro-, nano-, and ultrastructural features and molecular structures. Bone can dynamically adapt to local needs at each level of its multi-scale hierarchy, allowing the optimization of its material composition and structure to meet functional requirements. The tissue itself is made up of ~35-45% hydroxyapatite mineral crystals , ~40% organic matrix including type I collagen and other non-collagenous proteins, and ~15-25% water, by volume (Boskey and Robey 2018). These components combine to provide flexibility, toughness, and elasticity and can change independently, or together, due to aging and disease.

Hydration's essential role in bone across the material's hierarchy has become clear just over the past few decades. Although long accepted that water constitutes roughly a quarter of the cortical bone by volume (R. A. Robinson 1952; Neuman and Neuman 1958) and can be modulated *ex vivo* by temperature and solvents (Yan, et al. 2008; Nyman, et al. 2006), there is now a growing appreciation for how it can dynamically change due to age (X. Wang, et al. 2018), disease (Allen, et al. 2015a), and treatment (Gallant, et al. 2014). Bulk changes in total water display an inverse relationship with bone mineral content and strength (Elliott and Robinson 1957; Fernandez-Seara, et al. 2004). When water is completely removed, a bone has lower energy to fracture (Evans and Lebow 1951; Yamada and Evans 1970) and toughness (Evans and Lebow 1951; Sedlin and Hirsch 1966), higher hardness (Rho and Pharr 1999), tensile strength (Dempster and Liddicoat 1952) and stiffness (Rho and Pharr 1999; Evans 1973). Complete dehydration is not physiologically relevant, so understanding how small modulations of hydration, in both directions, and how they influence mechanics is important to understand.

A key emerging area related to bone mechanical and tissue properties lies in differentiating the role of water in its four different compartments, including ***free*** or ***pore water***, water ***loosely bound*** at the collagen/mineral interfaces, water ***tightly bound*** within collagen triple helices, and ***structural water*** within the mineral (**Figure 1**). Due to the advent of- and improvements to- techniques able to probe nano- and molecular scales, our knowledge of these compartments continues to grow from our original understanding (Dempster and Liddicoat 1952; Evans 1973), which relied on calorimetry of frozen bone tissue to derive total water (W. Robinson

1931). The foundational review of bone hydration conducted by Granke, Does, and Nyman in 2015 set the stage for the bone field to (re)consider hydration's value as a clinical biomarker for bone health and an attractive therapeutic target in reducing fracture risk (Granke, et al. 2015a). The current review will summarize our current knowledge of water across the four identified water compartments and how alterations to each phase relate to mechanical changes. We also discuss the current state of imaging and spectral techniques used to study bone water. Finally, we summarize how water changes in several disease states (e.g., chronic kidney disease, diabetes, osteogenesis imperfecta, osteoporosis) and how hydration can be therapeutically modulated.

2. Bone Hydration – The Four Functional Compartments

2.1. Free Water

Water in this compartment can flow freely within pores, vascular canals, central (Haversian/Volkmann) canals, and in the lacunar-canalicular network. It accounts for about 20% of total bone water (Biswas, et al. 2012). The literature uses "free" and "pore" water interchangeably, although the term 'free' seems more appropriate since the other compartments all refer to a characteristic of water binding, rather than a physical location within the bone. Mechanically, an increase in free water results in a loss of strength and stiffness with a small contribution to a loss in toughness (**Figure 2**). This is mainly due to the inverse relationship between bone mineral/mass and free water. Early studies using proton-deuteron exchange nuclear magnetic resonance (NMR) determined free water is exchangeable 1:1 with mineral; the more mineral in the system, the less porous the bone and the less free water (Wehrli and Fernandez-Seara 2005). This underpins using free water as a direct surrogate for cortical porosity. Ultra-short echo time (UTE) magnetic resonance imaging (MRI) can derive a "porosity index" values, using the fraction of bound and free water, which significantly correlates to cortical porosity measured via micro-computed tomography (μCT) ($r^2 > 0.8$, $p<0.001$) ((C. S. Rajapakse, et al. 2015).

The portion of free water not found within cortical pores is thought to play an important role in transmitting signal from cell to cell via streaming potential (Liu, et al. 2019) and/or as measured fluid shear stress by the osteocyte cell walls (Monteiro, et al. 2021; Moore, et al. 2018; Morrell, et al. 2018). In addition, this free water provides vital nourishment (glucose) to the cells (S. Wang, et al. 2021a) and participates in transport of solutes

from osteocyte-derived signaling molecules enclosed in the lacunar-canalicular system (order of 0.1-1 μm) (L. Wang 2018).

2.2. Loosely Bound Water

Bound water associated with mineral and/or collagen accounts for the remainder of bone's total water and can be categorized into three different compartments: loosely bound, tightly bound, and structural. Loosely bound water is located at the interface of the collagen fibril and mineral crystals resides within the organized layer of collagen molecules and mineral crystals (thickness: 0.160 nm without water, ~0.230-0.255 nm with bound water) and can be associated with collagen or mineral molecule (physical adsorption) (Lees 1981). Loosely bound water, about ~20% of cortical bone's wet weight (Ong, et al. 2012), positively correlates with organic matrix density (Cao, et al. 2008) and plays an essential role in transferring loads between collagen and mineral by allowing sliding at their interfaces. This action reduces shear stresses (Feng-Chao Wang and Zhao 2011) and increases overall tissue toughness (J. Samuel, et al. 2016a). When loosely bound water is removed by thermal dehydration, bone becomes less tough, illustrating its role in governing post-yield mechanical behavior (**Figure 2)** (Yan, et al. 2008; Nyman, et al. 2006; Nyman, et al. 2013).

The mineral charge found on the mineral crystal surface was once thought to be the only binding mechanism (Timmins and Wall 1977) to the highly dielectric water (Marino, et al. 1967). Recent work has pointed to the strong hydrophilic properties associated with the neighboring collagen molecules as another factor drawing water to these mineral-collagen spaces. Notably, the role of proteoglycans and their negatively charged glycosaminoglycans (GAGs), which have a great affinity for both collagen and mineral crystals (Best, et al. 2008; Hashimoto, et al. 1995), has been of interest for their potential role in retaining water in the matrix via their osmotic potential (X. Wang, et al. 2016). A loss of GAG is associated with loss of bone toughness, a reduction in bound water (X. Wang, et al. 2018), and a reduction in plastic energy dissipation in the extrafibrillar matrix (X. Wang, et al. 2016; Han, et al. 2021). When mice are supplemented with chondroitin sulfate (via injection), toughness and matrix bound water increase (Hua, et al. 2020), yet the efficacy of oral chondroitin sulfate supplementation in humans remains controversial (Henrotin, et al. 2010). Bone glycation reduces bound water

fraction (compared to non-glycated bone), suggesting matrix manipulations affect loosely bound water modulation (Nyman, et al. 2019).

The portion of loosely bound water bound to/associated with the mineral (Wilson, et al. 2005) correlates negatively with elastic modulus and positively to strength (Unal and Akkus 2015). When mineral-associated loosely bound water is removed by dehydration, loss of creep (rate of deformation under continuous load) is introduced into the system (Eberhardsteiner, et al. 2014). This mineral-related fraction of the loosely bound water may contribute to mineral crystal orientation along the length of crystal through interactions with the disordered and highly hydrophilic amorphous calcium phosphate layer (Y. Wang, et al. 2013; Faingold, et al. 2014) by trapping or binding water forming a hydration shell surrounding the mineral platelets (Von Euw, et al. 2018). The water molecules trapped at the amorphous calcium phosphate layer are thought to form hydration spheres serving as “place holders” for the ions to be incorporated into the solid phase (Von Euw, et al. 2018; Drouet C 2018). It is unknown whether these trapped water molecules contribute to the amorphization of the outer bone mineral itself (Von Euw, et al. 2018). The degree of adsorption of water molecules to hydroxyapatite deteriorates with age and disease (Vaissier Welborn 2021; Ivanchenko, et al. 2017).

2.3. Tightly Bound Water

The water fraction that is tightly bound to the collagen triple helix is found at amounts of ~0.5 grams of water per gram of collagen (Privalov 1958) and is positively associated with bone toughness and negatively with stiffness (Nyman, et al. 2006). The long fibrillar collagen structure can hold abundant water due to its shape (large surface area with high water affinity), yet it has been postulated that collagen is fibrillar because the bound water provides structure throughout this length. This is due to the observation that collagen type I structure will shorten upon water removal (Masic, et al. 2015). Within the tightly bound water pool, three distinct collagen-associated water compartments have been identified: single and double water bridges (between alpha helices too distant for direct hydrogen bonding), cleft water within the grooves of the triple helix, and water of the interfacial monolayer (Fullerton and Amurao 2006; Fullerton, et al. 2006). Water also determines collagen’s efficient functioning at temperatures (Trebacz and Wojtowicz 2005): dry proteins cannot unfold upon heating or

cooling thus the ability to denature due to temperature is likely caused by the presence of bound water in the system.

2.4. Structural Water

Structural water molecules are incorporated around the mineral lattice of the carbonated apatite structures themselves (Von Euw, et al. 2018; Yoder, et al. 2012). As its name suggests, structural water provides mechanical stability via bridges of hydrogen bonds between ions in the apatite crystal (Wilson, et al. 2005). This structural water acts as part of a bridge for the octacalcium phosphate citrate complex (Davies, et al. 2014) organizing the mineral platelets (Y. Wang, et al. 2013) while providing stability to the inherent crystal imperfections by filling vacancies (Wilson, et al. 2005). This mineral-mineral support is crucial because nearly 30% (Alexander, et al. 2012) - 70% (McNally, et al. 2012) of mineral structures are not in direct contact with collagen fibrils and thus the collagen fibrils themselves cannot serve as a template for organization. It is suggested that structural water provides a medium that allows mineral platelets to maintain organization and create a “continuous cross-fibrillar phase” within the winding volume between disordered collagen fibrils (Von Euw, et al. 2018; Reznikov, et al. 2018). Structural water may serve a role in regulating the accumulation or aggregation of mineral (Duer and Veis 2013).

3. Imaging and Spectral Methods to Quantify Bone Water

Bone’s high photoelectric absorption has made ionizing x-ray-based techniques the modality of choice to image the mineral phase of bone since the introduction of bone radiographs by Roentgen in 1895 (Mahesh 2013; Kanis 2002). It is well accepted that assessment of mineral (often by measuring bone mineral density (BMD)) is an incomplete index of fragility, accounts for only a fraction of bone strength (Hernandez and van der Meulen 2017), and may not adequately predict fracture risk (Kanis 2002; Marshall, et al. 1996; Tremollieres, et al. 2010). The extremely high resolution achievable by computed tomography (CT) and high-resolution peripheral quantitative CT (HR-pQCT) has allowed for detailed quantification of microstructural features of the mineral phase, including cortical porosity, giving insight into mechanical properties beyond BMD (Boughton, et al. 2019). Yet X-ray based techniques come at a price of ionizing radiation which has long-term health concerns (Lin 2010)

and can damage the very tissue we aim to image (Laperre, et al. 2011; Williams and Davies 2006). This limits its application in clinically vulnerable populations (children, cancer patients) and makes acquisition of multiple imaging timepoints less than ideal (Choksi, et al. 2018).

NMR spectroscopy and MRI represent the primary methods used to nondestructively study bone hydration (K. H. Mroue, et al. 2015; Saeed Jerban, et al. 2020a; Singh, et al. 2013). Compelling progress in solid-state NMR (ssNMR) has allowed us to study the direct relationship of bound water to a host of extracellular matrix components. Advancement in MRI technology has permitted spatially resolved quantification of water down to the tightly bound compartment *in vivo*. In addition, developments using "vibrational spectroscopy" (Raman spectroscopy, near infrared spectral imaging (NIRSI)) and photoacoustic imaging are positively altering the landscape of bone imaging and spectroscopy and continue to increase our understanding of bone's chemical composition and hydration across its discrete length scales.

3.1. Solid-State Nuclear Magnetic Resonance (ssNMR)

NMR spectroscopy is based on the spins of atomic nuclei; when radiofrequency waves are applied to molecules placed in a strong magnetic field, nuclei will resonate at a biologically specific frequency and emit energy, which is collected and converted to NMR spectra as the spins return to equilibrium. NMR has long been used to determine the structure of small molecules and large proteins in solutions. ssNMR is becoming an increasingly popular technique that can probe the microstructural details of biomaterials such as bone with pico-meter resolution in the tissue's absolute native state (Ong, et al. 2012; Murray, et al. 2013; Singh, et al. 2014; P. Fantazzini, et al. 2003; Paola Fantazzini, et al. 2004). Hardware updates coupled with technological advancement in ultra-fast magic angle spinning (MAS) methods has improved resolution and sensitivity of ssNMR by attenuating the broadening effects of dipolar couplings and chemical shift anisotropy (Brown 2012; Hodgkinson and Wimperis 2009), making the direct evaluation of amide regions, collagen, and their associated water molecules a possibility (K. H. Mroue, et al. 2015). The technique is credited with the discovery of structural water, which had not been determined until ssNMR studies of mineralized tissue were conducted (Wilson, et al. 2005; Casciani 1971). Numerous ssNMR experiments have efficaciously probed water across all four of its identified phases and are briefly discussed below. It is important to note that bone specimen preparation is vital

to the ssNMR experimental approach. Preparation of bone into a powder using chemical/physical treatment should be avoided due to the risk of perturbing internal features and bonds (Ratan Kumar Rai and Sinha 2011). Therefore, intact preparation methods, including breaking the bone into larger "chunks" or machining cylindrical rotor-shaped beams, are preferred for conducting ultra-structural studies in the native state (Singh, et al. 2013; Nikel, et al. 2012).

1D ^{1}H experiments changed the landscape of bone ssNMR (Granke, et al. 2015a; Wehrli and Fernandez-Seara 2005; R. A. Horch, et al. 2010). 1D ^{1}H acquisitions are the cornerstone of deriving total bone water content (R. A. Horch, et al. 2010; R. K. Rai, et al. 2013), resolving transverse (T_2) time constants (R. A. Horch, et al. 2011), and monitor diffusion (Wehrli and Fernandez-Seara 2005) which have been reviewed previously (Granke, et al. 2015a). More recently, ^{1}H experiments have been used to provide additional structural detail regarding matrix triglycerides (K. H. Mroue, et al. 2016) where lipid chains are shown to be significantly and negatively altered as a function of decreasing water content (Tiwari, et al. 2020), suggesting water may have an additional role stabilizing matrix triglycerides (**Figure 3)**. In combination with ^{1}H, ^{13}C chemical shift can detect conformational collagen changes (R. K. Rai, et al. 2015; Kamal H. Mroue, et al. 2012) and have highlighted water's influence on the mobility of amino acid residues in collagen on the periphery of the triple helix (Reichert, et al. 2004) and the presence of a hydrogen bonding network between GAGs in the collagen and mineral interface (P. Zhu, et al. 2009a). The ^{13}C[^{31}P] rotational echo double resonance (REDOR) technique can calculate the distance- and amount of bound water between collagen side-chain residues and the inorganic surface. REDOR experiments have demonstrated the distance between collagen and mineral crystal decreases with decreasing hydration (R. K. Rai, et al. 2013), increasing age (Nikel, et al. 2012), and in states of bone loss (R. K. Rai, et al. 2013). Finally, 2D ^{1}H-^{31}P heteronucleation correlation (HetCor) experiments, based on the distance-dependent heteronuclear dipolar coupling between phosphate and hydrogen, can be used to measure bound water content relative to inorganic content. 2D HetCor was used to document, for the first time, the presence of structural water in three different locations: occupying vacancies within mineral crystal apatite, in the internal portion of the mineral crystal, and at the mineral surface (Wilson, et al. 2006). When used in experiments of bone healing, ^{1}H-^{31}P HetCor was able to document the earliest stages of biomineral formation (and associated water changes) including the size and shape of mineral apatite (Vyalikh, et al. 2017) and, in preclinical studies HetCor

has shown it can differentiate bound water with treatment (R. K. Rai, et al. 2013). Although a powerful tool, ssNMR has limitations. First NMR and ssNMR cannot be acquired *in vivo,* and the technique cannot spatially resolve water compartments. Further, ssNMR requires specialized hardware to achieve MAS limiting its widespread use.

3.2. Magnetic Resonance Imaging (MRI)

MRI is a powerful non-invasive, non-destructive technique which continues to gain interest in bone applications for its sensitivity to biochemical composition and its rich dynamic range. The premise of MRI was born from the basic principle of NMR; (typically) MRI is used to detect ^{1}H nuclei from the water molecules present in a tissue. A radiofrequency pulse (RF) is applied, the protons are stimulated, spin out of equilibrium and, when the RF pulse is removed, return to equilibrium where the energy signal is detected and undergoes a Fourier transform to resolve the image (Mastrogiacomo, et al. 2019). MRI is acquired without the use of ionizing radiation, permitting safe longitudinal studies where multiple X-ray based imaging acquisitions would be unfeasible and potentially unsafe (Damilakis, et al. 2010). Compared to NMR, MRI can spatially resolve biochemical information and can be acquired *in vivo***.** Yet in conventional MRI, bone appears as a signal void and is unable to capture the tissue's inherently ultra-short transverse relaxation time (T_2) which is dictated by bone's limited hydrogen pool. This is because echo times (TE), or the time between RF excitation and signal acquisition, are too long (a few milliseconds or longer) and most protons from bone's limited water compartments have relaxed before signal is acquired (R. A. Horch, et al. 2010). More specifically, proton signal intensity is drawn from its water phases with ultra-short T_2 values coming from pore water protons (T_2>1 ms), loosely bound water protons (T_2=300-400 μs), tightly bound water (collagen backbone/sidechain, T_2<<20 μs), and structural/mineral water (T_2<<10 μs) (Nyman, et al. 2006; Granke, et al. 2015a; R. A. Horch, et al. 2010; Nyman, et al. 2008). Remarkable advances, however, have been made to evaluate bone water's inherently short T_2 components including the advent of three different clinically attractive short T_2 sensitive MRI methods: ultrashort echo time (UTE) (Robson and Bydder 2006; Siriwanarangsun, et al. 2016), free induction decay (FID)-projection otherwise known as zero echo time (ZTE) (Hafner 1994; Madio and Lowe 1995; M. Weiger, et al. 2011), and SWeep Imaging with Fourier Transformation (SWIFT) (Idiyatullin, et al. 2006).

UTE is by far the most widely implemented in this class of sequences and can be found on most clinical MRI scanners streamlining its accessibility including implementation into clinical research (Y. J. Ma, et al. 2020a).The current state of UTE-MRI can detect implicit signal from free water, matrix loosely bound water, and total water with precision, yet the conventional UTE evaluation of tightly bound or structural water have proven difficult due to restrictions in achieving a nominal T_2 associated with tightly-bound water compartments. Therefore, a broader range of techniques are being explored including the development of 3D-UTE Cones imaging combined with magnetization transfer, ZTE, and SWIFT and Multi-band SWIFT (MB-SWIFT) to resolve the tightly bound pools. Direct measures of the structural water fraction via MRI remains challenging, but if achieved, the spatial information regarding structural water concentrations would represent a significant payoff. While MRI continues to move the field forward through its non-invasive *in vivo* capabilities; compared to CT, proton-based MRI remains limited by the *in vivo* spatial resolution achievable while maintaining a sufficient signal-to-noise ratio.

3.2.1. UTE-MRI Loosely Bound and Free Water

Because the T_2 of loosely bound water is nearly ten times shorter than free water, multicomponent UTE-MRI fitting schemes are used to estimate contributions of (but not absolute proton content) loosely bound and free water. Several studies have elucidated that UTE- multicomponent-derived bound water relates to matrix density while free water confers to cortical porosity (Fernandez-Seara, et al. 2004; Nyman, et al. 2013; R. A. Horch, et al. 2011; Nyman, et al. 2008; W. C. Bae, et al. 2012a). UTE-MRI-derived free water varies regionally (**Figure 4)** (Zhao, et al. 2017), has a strong inverse relationship with bending strength and positively correlates to μCT-derived porosity (Manhard, et al. 2016; Won C. Bae, et al. 2012b), while bound water negatively correlates to porosity and ultimate stress (W. C. Bae, et al. 2012a). Bicomponent T_2 fitting analysis can detect bone porosities below ranges detectible by μCT and correlates with histomorphometric porosity measures (Saeed Jerban, et al. 2019a). However, bicomponent schemes can become less sensitive at high field strengths (7T) (Seifert, et al. 2015). Tricomponent fitting schemes using UTE acquisitions have been introduced which eliminate contribution of fat chemical shift to improve upon estimations of loosely bound and free water (Li, et al. 2015; Lu, et al. 2019; Saeed Jerban, et al. 2020b). Using human donor bone cortical strips, higher correlations of tricomponent vs. bicomponent bound and free water were found between microstructural (μCT) and

mechanical properties (via 4 point bending test) (Saeed Jerban, et al. 2020b) and tricomponent fitting reduced bound water overestimation which occurs near the endosteal surface (Lu, et al. 2019). All multicomponent T_2 fitting (analysis) requires collecting a series of echo times, the more echo times the better the exponential fit. Thus, scanning times for these studies can become lengthy (>>10-45 minutes). More recently, direct UTE measures of loosely bound and free water have been obtained though technology advancement. Bound water can be directly imaged using an adiabatic inversion recovery UTE (IR-UTE) which nulls the signal from the long T_2 components (R. Adam Horch, et al. 2012). Conversely, a direct measure of pore water is possible using double adiabatic full passage pulse UTE which uses a preparation pulse to saturate signal from bound water (making it null) followed by a UTE acquisition (Manhard, et al. 2015). Both the IR-UTE and double adiabatic full passage pulse UTE can be acquired using most clinical scanners. Choosing an appropriate minimum TE when evaluating bound water critical to prevent loss of signal from the bound pools; for example, a TE of 50 μs will result in a 1% signal loss of the free water component and a 14% signal loss from the bound water phase (Seifert and Wehrli 2016; Eric Y. Chang, et al. 2015a). This highlights that accurate evaluation of bone water protons by MRI requires an understanding of the biologically different relaxation times within the cortical bone across species, age, and disease, the use of an appropriate phantom, and an understanding of coil sensitivity and radiofrequency pulse durations, flip angles, and inhomogeneity of the system (Du, et al. 2010; Ya-Jun Ma, et al. 2020b). For more information regarding the technical aspects of UTE and the current state of UTE imaging as it relates to bone, the reader is referred to the thorough review by Ma *et al.* (Ya-Jun Ma, et al. 2020b).

3.2.2. MRI-derived Porosity Index

A singular dual-echo 3D UTE acquisition can be used to calculate the porosity index, a surrogate of cortical porosity based on the measure of free water (the signal ratio between a short (<50 μs) and longer (~ 2000 μs) TE acquisition). To obtain porosity index, the first echo is acquired using a TE which can capture signal associated with both loosely bound and pore water (total) and the second echo is at a time which captures only the signal arising from pore water (missing the ultra-short relaxation time of bound water). The UTE MRI-derived porosity index biomarker was first described in 2015 by Rajapakse and colleagues and has demonstrated strong positive correlations to μCT-derived porosity (r^2=0.79, p<0.001), pore size (r^2=0.81, p<0.001), and UTE-derived pore water fraction (r^2=0.62, p<0.001) and negatively to bone density measured via peripheral quantitative

computed tomography (pQCT, r^2=0.49, p<0.005) (C. S. Rajapakse, et al. 2015). Further, the non-ionizing measure of porosity can be acquired *in vivo* at clinically relevant field strength, and the acquisition is fast compared to multicomponent fitting schemes making clinical translation attractive (< 10 min) (**Figure 5A)** (C. S. Rajapakse, et al. 2015; B. C. Jones, et al. 2021). Follow up work has demonstrated that the porosity index is correlated to tibial stress (E. Y. Chang, et al. 2015b), is correlated to bone stiffness (r= -0.82, p=0.0014 (B. C. Jones, et al. 2021) – r= -0.79, p=0.002 (Hong, et al. 2019)) (**Figure 5B)**, accounts for ~63% of the variability in bone stiffness in the tibia (Hong, et al. 2019), and the measure has an inverse relationship to bound water and phosphorous content measured by both MRI and near infrared spectroscopy (**Figure 5C)** (Zhao, et al. 2017; Hong, et al. 2019).

3.2.3. MRI-derived Tightly Bound Water

The direct measure of the collagen backbone protons (tightly bound) in native bone tissue remains challenging using conventional UTE MRI (due to limitations in achieving a near-zero TE) thus alternative MR sequences have been explored. ZTE approaches can achieve a TE=0 by turning on the projection gradients prior to radiofrequency excitation using a large bandwidth hard pulse and 3D radial center-out encoding schemes. ZTE can provide higher spatial resolution and improved signal to noise ratio compared to UTE (Markus Weiger, et al. 2012) because spatial encoding starts without a delay at the full k-space speed. Yet implementation of ZTE is not always feasible because of hardware constraints required to achieve its acquisition parameters. Nevertheless, ZTE has been used in a proof-of-concept study to derive T_1 relaxation time from collagen-related water pools in mice *in vivo.* Results report a T_1 of 213± 95 ms belonging to collagen-bound water which represented a collagen bound water fraction of 7.4% in the mouse femoral diaphysis (Marcon, et al. 2017).

A technique called magnetization transfer (MT) combined with UTE-MRI and UTE-MRI multispoke Cones sequences has been deployed as a method to *indirectly* measure bone's collagen proton phase (E. Y. Chang, et al. 2015b; Ya-Jun Ma, et al. 2018; Ya-Jun Ma, et al. 2016). A benefit of this technique is that it can be conducted using most clinical scanners at clinically utilized field strength. To determine collagen associated water using MT, a two pool magnetization transfer works by transferring a saturated magnetization across protons from macromolecules to water protons which is then detected by the UTE-MRI to derive the

macromolecular proton fraction (estimate of collagen associated water) as well as exchange rates. If an additional UTE sequence is acquired to capture total water, an absolute measure of the collagenous matrix coined 'macromolecular proton density' can be estimated from the MT-UTE macromolecular proton fraction and the conventional UTE total water fraction (Saeed Jerban, et al. 2019b). The macromolecular proton density can be capture *in vivo* along with total, pore, and bound water, and is shown to decrease with age in volunteers (**Figure 6A,B).** When captured *ex vivo,* the macromolecular proton density of donor femora showed strong, significant correlation with female donor age (r=-0.91, p=0.03) and moderate to strong correlations with μCT-derived cortical porosity and BMD (r=-0.67, p<0.01 and r=0.65, p<0.01, respectively) (**Figure 6C**). It is assumed this measure represents bone collagenous matrix spatial distribution, by exploiting tightly bound collagen water, and could be potentially used to localize or "map" injury or mechanically weak spots in the matrix (Saeed Jerban, et al. 2019b), but work to validate this against spectral techniques (composition) and mechanical outcomes will need to be performed.

3.3. Vibrational Spectroscopy Techniques

3.3.1. Raman Spectroscopy

Raman spectroscopy is a non-destructive spectroscopic technique which relies on elastic scattering of photons (Rayleigh scattering) to detect vibrational and rotational states, chemical structure, and phase in biological systems (Robin R. Jones, et al. 2019). Raman has proven efficacious probing the biochemical composition of bone including the spectroscopic observation of mineral phosphate, carbonate, and matrix collagen (Bergholt, et al. 2019; Morris and Mandair 2011), their mechanical relationships (Makowski, et al. 2017), and even matrix lipids and phospholipids (Penel, et al. 2005). Raman permits the use of fresh tissue (in addition to fixed and embedded tissue), and tissue that has been stained or fluorescently labeled (allowing for analysis during period of treatment/rapid bone growth) (Donnelly, et al. 2010). Commercial Raman systems lack the sensitivity to resolve the OH-stretch band range, so custom short-wave infrared (SWIR) systems have been designed to achieve the sensitivity necessary to identify both water compartments and to which molecule they are bound to (Unal, et al. 2014). Using the SWIR technology, four OH-stretch band peaks have been identified through dehydration experimentation including: collagen related water at peak 3220 cm^{-1}, NH groups (collagen

backbone) and their related water at peak 3325 cm^{-1}, water associated with OH of hydroxyproline next to collagen water at 3453 cm^{-1}, and mineral-mineral (OH) water at 3584 cm^{-1} **(Figure 7A)** (Unal, et al. 2014). Based on the rate these four peaks were replaced by deuterium oxide, Unal *et al.* defined four spectroscopic biomarkers: I_{3220}/I_{2949}, I_{3325}/I_{2949} and I_{3453}/I_{2949} reflecting collagen-related water phases and collagen portion of bone while I_{3584}/I_{2949} reflects mineral-related water and the mineral portion of bone. Using serial Raman collections throughout dehydration, the authors observed Raman collagen-associated water (I_{3220}/I_{2949} and I_{3325}/I_{2949}) positively correlated with toughness (r^2=0.81 and r^2=0.79, both p<0.001) and post-yield toughness (r^2=0.65 and r^2=0.73, both p<0.001) while mineral related water (I_{3584}/I_{2949}) positively conferred to strength (r^2=0.46, p<0.001) and negatively to elastic modulus (r^2=0.78, p<0.001) via 3 point bending test (**Figure 7B-E**) (Unal and Akkus 2015). Work by others reported an increase in loosely bound water is observed with an increase in Amide I subpeak ratio which is related to collagen I's helical structure (Nyman, et al. 2019) pointing to the strength of Raman-based measures in providing information about the moieties in which water molecules are attached.

3.3.2. Near-Infrared Spectral Imaging (NIRSI)

NIRSI is a fast spectral technique which measures signals from molecular vibrations following incident radiation of the sample. For bone, NIRSI is particularly proficient at imaging organic components such as collagen and fat content as well as the spatial distribution of water (Gregory Chang, et al. 2017). For preparation of the sample, NIRSI is non-destructive and can measure intact samples with limited or no preparation including no chemical reagents (Chamith S. Rajapakse, et al. 2017) which contrasts with other traditional methods of biochemical analysis. Another benefit of NIRSI is its ability to image at high frequencies which allows for greater depth penetration (on the order of mm to cm) which makes it optimal for probing bone's cortex. NIR water absorbances included three currently identified peaks at 5152, 6560 and 7008 cm^{-1} (Ramyasri Ailavajhala, et al. 2019). NIRSI can provide additional, direct measures of matrix components such as collagen in addition to water. NIRSI collagen matrix (4608 cm^{-1}) peak correlated to NRISI water peak (7008 cm^{-1}) (r=0.69, p=0.004) and NIRSI water peaks at 5152 and 7008 cm^{-1} correlated to free and bound water derived from UTE (free: r=0.735, p=0.016 and bound: r=0.71, p=0.01) (Chamith S. Rajapakse, et al. 2017). One challenge in evaluating water content using spectral techniques is the risk of dehydration, or even rehydration due to atmospheric humidity, occurring during data acquisition hindering interpretation and reproducibility among other things. Ailavajhala *et al.* describe

the application of an environmentally controlled chamber for NIRSI to increase repeatability of cortical water measures without the influence of atmospheric moisture (Ramyasri Ailavajhala, et al. 2019). Using NIRSI collected in cortical bone at size different lyophilization time points, they were able to use a partial least squares model to generate a water calibration curve (in good agreement with gravimetric assessment). They reported peak 6560 cm^{-1} becomes insignificant following 48 hours of dehydration and any remaining water absorbances are likely to reflect tightly bound water (Ramyasri Ailavajhala, et al. 2019) but more work needs to be conducted to validate this observation.

3.4. Photoacoustic (PA) Imaging

PA imaging detects the acoustic signal triggered by infrared light irradiation to provide high-resolution optical images giving way to parameters such as molecular content depth and absorption coefficients (Xia, et al. 2014). Specifically, the pulsed infrared light is absorbed by the biological material which generates ultrasound waves on the principal of thermoelastic expansion. These ultrasound waves are collected by an ultrasound transducer and 3D images of optical absorption contrast are derived (Beard 2011). Those tissues considered "optical absorbers" such as blood and bone water are ideal for PA imaging where PA imaging can overcome limitations when using ultrasound alone (where the collected signal is that which is reflected from the tissue layers thus limiting the achievable penetration depth). PA imaging can be acquired *in situ, ex vivo*, and *in vivo* (Park, et al. 2020) although *in situ* and *ex vivo* is often optimal due to competing signal with surrounding blood flow. The molecular vibrational state of water is affected based on whether it is bound or unbound in a tissue. Since water can absorb electromagnetic waves found within the radio frequency and microwave spectra, it is a powerful absorber using radio frequency-based PA (otherwise referred to as thermoacoustic PA). More recently, work has demonstrated the potential of a near-IR based PA imaging to detect water spectra (Xu, et al. 2010) using a light source, but thermoacoustic PA remains the primary technique in bone thus far. In bone applications, PA imaging has been performed to obtain chemical information from the mineral, collagen, lipid, oxygenated and deoxygenated hemoglobin, and has even described a PA-derived BMD measure in good agreement with BMD measured using conventional approaches (Lashkari and Mandelis 2014; Feng, et al. 2015; Feng, et al. 2020; Feng, et al. 2021). Recent work used PA imaging to characterize absorption frequency from water, collagen, and lipids in osteoporotic and control rabbit bone. Using the relative content, PA demonstrated significantly

decreased collagen, increased lipid, and no change for relative water content between osteoporosis and control groups (Feng, et al. 2021). While there were no significant changes to water between groups, data presented the feasibility of PA imaging to derive water in bone for the first time. Initial results are promising as PA is a low-cost, non-ionizing and patient-friendly method that can provide information regarding the organic and nonorganic bone tissue and may prove to be a method that can provide a more “complete” picture of bone health.

4. Bone Water with Age and Disease

BMD almost universally falls short across disease state in predicting fracture risk and fracture resistance. Therefore, a biomarker such as bone hydration, that can predict additional aspects of bone health, represents a potential clinical tool that could complement BMD in assessing bone disease and treatment efficacy. Work has been conducted characterizing bound and free water in aged and osteoporotic bone, including correlating how free water relates to cortical porosity. More recently, studies have applied UTE-MRI, ssNMR, NIRSI, and Raman spectral techniques to understand how alterations in hydration with aging and diseases such as chronic kidney disease, diabetes, and osteogenesis imperfecta relate to mechanical outcomes.

4.1. Aging

Fracture risk increases in the aging skeleton; nearly 50% of women and 25% of men will sustain a fracture after 50 years of age (Sheer, et al. 2020). When an aged bone fails, the fracture is characterized by a reduced strain at failure and a more linear crack pattern (Nyman, et al. 2013; Koester, et al. 2011; Katsamenis, et al. 2015). Historically, reduced bone strength was thought to result from lower bone mass, density, and alterations to skeletal architecture. These factors can only explain ~75% of increased fracture risk due to age, and increased fragility is often observed with a disproportionate loss in mass, trabecular reorganization, or decreased BMD (Burr and Turner 1999; Hui, et al. 1988; Kanis, et al. 2001). Recent work has illuminated age-related changes in bone water within the extracellular matrix including increased free water, decreased bound, and alterations to the water residing on the collagen backbone.

Total water under normative conditions can range between 10-20% of total cortical volume and drop to 5% by the 6th decade of life (R. A. Robinson 1952; Neuman and Neuman 1958). Total water proton density

measured via UTE-MRI correlates significantly with BMD (r=0.71, p<0.01) in aged human donor samples (61 ± 24 yrs old) (S. Jerban, et al. 2020c). However, relying on bulk water to predict fracture risk in the aged skeleton is likely insufficient. Horch *et al.* demonstrated that free water had strong negative correlations and bound water strong positive correlations with peak stress while bulk water did not correlate with the measure (R. A. Horch, et al. 2011). Numerous MRI-based studies indicate that free water increases with aging, and MRI-derived free water positively correlates with μCT-derived cortical porosity (Wehrli and Fernandez-Seara 2005; C. S. Rajapakse, et al. 2015; Chamith S. Rajapakse, et al. 2017; Akbari, et al. 2016). The strength of free water as a non-invasive marker of cortical porosity has been exploited in the aging skeleton using the MRI-derived porosity index as a non-ionizing method to track microstructural matrix alteration. In aged specimens, porosity index positively correlates with increased number and size of pores and direct measures of pore water using UTE-MRI and NIRSI (C. S. Rajapakse, et al. 2015; E. Y. Chang, et al. 2015b). In aged donor specimens (72.1 ± 15.0 yrs old, ten male, five female), UTE-MRI porosity index measured at the cortical shaft significantly correlated with whole bone stiffness (r=-0.82, p=0.0014) calculated using a mechanical test mimicking a sideways fall (B. C. Jones, et al. 2021). Notably, multiple regression analysis demonstrated that porosity index was a strong predictor of bone stiffness independent of volumetric BMD and cortical thickness indicating its value in predicting whole-bone mechanical integrity. While free water appears to be a viable biomarker in this context, its value largely lies in its ability to predict porosity with less clarity around the specific impact on free water.

Bound water is vital to maintaining bone toughness and strength (Peizhi Zhu, et al. 2009b; Jitin Samuel, et al. 2016b), both of which are reduced with age (Nyman, et al. 2013; R. A. Horch, et al. 2011; Granke, et al. 2015b). Bound water is nearly 40% lower in elderly cadaveric specimens (73 ± 5 yrs) compared to young specimens (26 ± 6 yrs), accounting for upwards of 70% of the age-associated lower bone toughness **(Figure 8A-C)** (X. Wang, et al. 2018). Bound water loss and decreased toughness are often seen with collagen derangements suggesting a coadjuvent relationship where changes may be successive or concurrent steps in aging. Advanced age in BALB-c mice (20 mo) is associated with significantly lower femoral toughness, fracture toughness, and matrix bound water (via ^{1}H NMR), and higher enzymatic (mature hyroxylysyl-pyridinoline) and non-enzymatic crosslinking (pentosidine) and Amide I sub-peak ratio (via Raman) (Creecy, et al. 2020). Increased Amide I sub-peak ratio may help explain decreased bound water due to diminished hydrogen bonding

sites between residues of collagen and surface mineral crystal. Similar extracellular matrix compositional changes (higher AGEs and cross-linking) and lower bound water were observed alongside lower fracture resistance in aged (24 mo) male Fischer F344 rats (Uppuganti, et al. 2016). As a result of these and other works (Bridelli, et al. 2017; Jazini, et al. 2012), it is hypothesized that loss of bound water and increased glycation are related and consequential steps during aging. While it is not entirely clear, evidence supports a loss of bound water may initiate glycation events (Bridelli, et al. 2017) while increased cross-linking may physically displace existing or prevent new bound water (Kopp, et al. 1989).

4.2. Osteoporosis

Osteoporosis represents a systemic metabolic skeletal disorder marked by altered bone remodeling leading to reduced bone strength and increased fracture risk (Lorentzon and Cummings 2015). BMD has long served as a diagnostic measure for osteoporosis where the disease is characterized by a BMD which falls below -2.5 standard deviations for the mean BMD of normal young females (Kanis 1994). Porosity index in postmenopausal women has been shown to range from 15-38% (C. S. Rajapakse, et al. 2015). More recently, work has been conducted to evaluate relationships between age and body mass index (BMI) among pre- and postmenopausal women. Porosity index (%) measured at the tibia in pre- and postmenopausal female volunteers (45.7 ± 15.9 yrs) using UTE-MRI was positively correlated with age in postmenopausal but not premenopausal women and negatively correlated with BMI in both groups (Chen and Yuan 2018). These correlations were not observed when porosity index was calculated at the femoral neck, a common fracture site in osteoporosis. Interestingly, porosity index at the tibia and femoral neck were not correlated suggesting important region-dependent alterations to porosity and bone water are present.

In a recent study, Raman spectroscopy was acquired in iliac crest biopsies collected from postmenopausal women who have sustained a fracture and compared to age- and BMD-matched non-fracturing postmenopausal women (Rokidi, et al. 2019). Women who had sustained an osteoporotic fracture demonstrated significantly decreased tissue water as well as lower GAG, higher pyridinoline (enzymatic collagen cross-link), and higher N(6)- carboxymethyllysine (an AGE). The greatest difference between fractured and non-fracture controls came from the Raman measure of tissue water. Mechanically, these changes result in significantly lower

hardness and modulus via nanoindentation (Vennin, et al. 2017). Results in this cohort of age- and BMD-matched bone strongly suggest water could serve as an independent determinant of fracture risk. While measures were not derived using *in vivo* techniques, they were calculated from iliac crest biopsy which is a standard, although invasive, method for obtaining clinical biopsy suggesting further studies could be utilized validating biopsy results with *in vivo* findings (using UTE-MRI, for example).

Ovariectomized (OVX) animals have long served as a preclinical model to study postmenopausal osteoporosis. Using SWIFT MRI in a cross-sectional study design, cortical bone water signal intensity was significantly higher by 8 weeks post-OVX surgery compared to SHAM controls (Sukenari, et al. 2015). MRI-based measures of signal intensity were positively correlated with new bone area measured using histomorphometric analysis, but no correlation was found with BMD. In the only study to date applying *in vivo* MRI-based measures to follow disease progression, SWIFT-MRI was used to quantify cortical water, cortical matrix T_1 relaxation times (a tissue-specific biomarker where measures are related to tissue organization), and marrow fat content at baseline and 2, 4, 10 and 12 weeks post-OVX (Surowiec, et al. 2021). By week 10, SWIFT detected a significant decrease in cortical water and T_1 relaxation times, indicative of a more disorganized matrix with reduced bound water, and a significant increase in marrow fat content consistent with postmenopausal osteoporosis. However, bi- or tri- component analysis was not conducted in either study thus the authors could not distinguish which water compartment(s) were driving OVX-related changes.

4.3. Chronic Kidney Disease

Kidney injury or disease can catalyze a cascade of biological events involving numerous pathophysiological pathways that have prominent and deleterious effects on the skeleton. CKD patients have a 2-14-fold greater fracture risk than the age-matched healthy population which increases with disease progression (Nickolas, et al. 2008). Susceptibility to fracture appears well before the need for dialysis and cannot be fully explained by changes in bone mass and BMD. There is a growing body of pre-clinical literature documenting alterations in matrix tissue properties (collagen, hydration) which are linked to bone brittleness and are also present in CKD (Mitome, et al. 2011; Iwasaki, et al. 2015; Newman, et al. 2014).

The male Cy rat model of progressive CKD has a bone phenotype that includes significantly increased cortical porosity (McNerny, et al. 2019) and severely diminished mechanical properties compared to normal littermates (Newman, et al. 2014). At the material level, modifications in collagen crosslinking and bone hydration are present and are differentially affected in high- and low-turnover subtypes (driven by parathyroid hormone (PTH)) of the disease (Allen, et al. 2015a). Compared to normal littermates, high-turnover (high PTH) CKD rats had cortical bone with lower bound water and higher pore water; low turnover (low PTH) CKD rats had cortical bone with higher bound water and lower pore water (**Figure 9A**) (Allen, et al. 2015a). Serum PTH correlated positively to pore water and negatively to bound water (**Figure 9B,C)**. Pore water tracked closely to changes in cortical porosity, which was higher in high-turnover animals and lower in low-turnover animals at 35 weeks. Bound water was observed to be inversely related to mineralization. Notably, at 30-weeks, mineralization was largely unchanged (measured by Raman spectroscopy) in high turnover animals yet bound water fraction (by UTE-MRI) was significantly lower. Because significant changes in cortical porosity were not observed, it is plausible that alterations in bound water at the mineral/collagen interface may preceded changes in bulk mineralization serving as an earlier event or biomarker in the cascade of CKD-associated skeletal derangements.

4.4. Diabetes

Diabetes is a chronic, complex metabolic disorder with wide-reaching clinical manifestations. Under diabetic conditions, patients can have increased fracture risk, delayed fracture healing, and impaired bone formation (Vestergaard 2007). Diabetic patients typically present with normal or even high BMD coupled with low bone turnover which cannot explain the high rate of facture (Farr and Khosla 2016). Thus, diabetes represents a paradoxical bone disorder where normative or high BMD is coupled with compromised bone quality leading to poor mechanical outcomes.

Raman-derived tissue water content (based on nanoporosity; calculated from the ratio of integrated spectral slice 494–509 cm^{-1} (PMMA to Amide III) was measured in tetracycline labeled iliac crest biopsies from premenopausal women with Type 2 diabetes (Rokidi, et al. 2020). Actively forming cortical bone nearest to the osteon demonstrated the greatest water content which decreased significantly as a function of tissue age determined by tetracycline labels. Biopsies were fixed in ethanol thus analysis of water peaks as described by

Unal *et al.* (Unal and Akkus 2015) could not be conducted. Tissue-level assessment in patients with Type 1 diabetes remains limited.

SWIFT MRI (using a TE~0) could detect changes between diabetic and control male Wistar/ST rats two weeks following streptozotocin (STZ) injections to induce T1D, where changes in BMD were not detectable until week eight (Minami, et al. 2018). At two weeks post STZ, mechanical properties including stiffness and energy absorption were significantly compromised and bone formation measured via histomorphometry was suppressed. Proton-based MRI-SWIFT measures, which could detect diabetic-induced bone changes in the matrix four week prior to changes in BMD by μCT, suggest matrix water is altered before bulk mineral manifestations are detected.

4.5. Osteogenesis Imperfecta

Osteogenesis imperfecta (OI) is a rare and severe heritable collagen-based bone disorder characterized by low bone mass and pore bone quality and increased fracture risk (Van Dijk and Sillence 2014). OI is both a genetically and clinically heterogeneous disease that can differ in modes of inheritance and phenotypic presentation ranging in severity from mild forms to perinatally lethal (Marini, et al. 2017). Research has largely been focused on the material level property changes directly associated with the altered collagen followed by a focus on the poor mineral quality (Surowiec, et al. 2020; Camacho, et al. 2003). Water, particularly loosely and tightly bound collagen-related water, is hypothesized to play a role in governing bone health in OI through supporting formation and maintenance of collagen structure and possibly mineralization (Kramer, et al. 2000; R. Ailavajhala, et al. 2020). Despite this link, little is known about how bone water is altered under OI conditions. The first mention of bone water in OI came in 2002 where structural modeling suggested that tightly bound water molecules may be increased in OI to help compensate for lost solute hydrogen bond stability observed at the collagen level when OI-causing mutations affecting the *COL1A1* gene are present (Mooney and Klein 2002).

In pre-clinical testing, NIR spectral analysis in the *oim/oim* (OIM) mouse model of moderate-to-severe OI demonstrated that cortical bone had a 50% higher overall water content in OIM compared to wildtype controls (**Figure 10A)** (Shanas, et al. 2021). The authors postulate this was a result of more matrix space in OIM bone for water to 'loosely associate with'. The tightly bound water pool, when considered relative to total matrix content,

was higher in OIM mice compared to controls which was negatively correlated with stiffness (r=-0.44, p<0.05) and maximum load (r=-0.60, p<0.05) suggesting the presence of higher mineralization content (**Figure 10B-D)**. Similar findings of higher bound have been reported in the OIM mouse vs. wildtype when atomic force microscopy (AFM) imaging and cantilever-based nanoindentation was carried out in hydrated and dehydrated collagen fibrils (Andriotis, et al. 2015). Under air dehydration, the OIM collagen fibrils had lower indentation modulus, greater intermolecular space, and higher remaining water content compared to wildtype collagen fibrils. Because air-dehydration can remove free water, the remaining water represents loosely bound, tightly bound, and structural water. Upon re-hydration in saline, OIM fibrils had a higher indentation modulus (14.2 vs. 2.8 MPa, p<0.001) and decreased fibrillar swelling (42% lower, p<0.001) compared to wildtype. The authors hypothesized the higher remaining bound and structural water content observed during air-dehydration experiments left less room for a further increase to bound water upon rehydration perhaps due to an 'increase of non-enzymatic cross-linking resisting fibril dilation' observed in previous work.

5. Bone Hydration as a Therapeutic Target

Current treatment paradigms for reducing fracture risk are focused on building more bone by increasing osteoblast activity or reduce the rate of bone loss through osteoclast inhibition. While these approaches have been effective, they have limitations (Seeman 2017). Anti-resorptive agents are the most widely used therapeutic to improve BMD and reduce fracture yet long-term use has been implicated in negative bone quality outcomes. This occurs in part because the suppression of remodeling leads to continual changes in both the mineral and collagen phases, imparting effects that tend to embrittle the matrix, such as increased non-enzymatic collagen crosslinking, microdamage accrual, and increased mineral heterogeneity (Gourion-Arsiquaud, et al. 2010; Allen, et al. 2008). Each of these effects is known to correlate to poorer mechanical outcomes (Allen and Burr 2011; Acevedo, et al. 2015). Therapeutic modulation of water, specifically the bound water fraction, represents a novel approach to improve mechanical properties and reduce fracture risk. To date, most of the therapeutic work related to hydration has utilized Raloxifene.

Raloxifene is a selective estrogen receptor modulator (SERM) that functions as an estrogen agonist in the skeleton due to predominant interactions with estrogen receptor alpha (ERα) over ER beta (ERβ) (which would lead to antagonist effects) (Rey, et al. 2009). Raloxifene is the generic name for 1-[6-hydroxy-2-(4-hydroxyphenyl)benzo[b]thien-3-yl]-1-[4-[2-(1-piperidinyl)ethoxy]phenyl]methanone (**Figure 11A)**. It has been approved for use since 1997 in the US and 1998 in Europe for the treatment of osteoporosis and as a result of nearly 20 years on the market, has amassed a great deal of data regarding its safety and efficacy. Clinical treatment with RAL has demonstrated significant decreases in fracture risk (~50%) while only modestly suppressing bone remodeling and minor increases to BMD suggestive of bone quality changes beyond the mineral acting to improve mechanical properties (Ettinger, et al. 1999; Riggs and Melton 2002; Sarkar, et al. 2002). Post-menopausal women treated with RAL demonstrated a concurrent increase in total body water, raising the potential that bone water may increase, too (Jacobsen, et al. 2010).

Raloxifene has been shown to directly interact with the bone matrix in a cell- and estrogen independent manner (Gallant, et al. 2014; Bivi, et al. 2016). Non-viable canine bone beams soaked in a solution of raloxifene demonstrated a significantly higher level of matrix bound water (via UTE-MRI) while small angle X-ray scattering during four-point bending showed that raloxifene transferred load between collagen and mineral crystals resulting in lower strain on the mineral and greater overall deformation (Gallant, et al. 2014). Further, observations showing increased collagen-D periodic spacing following raloxifene exposure suggest the potential of swelling occurring within the collagen fibrillar structure likely a result of the increased bound water. Using NMR and Fourier transform infrared spectroscopy (FTIR), it was revealed that raloxifene interacts with collagen, collagen/mineral, but not mineral alone and that the interaction is done through its basic sidechain (**Figure 11B-D)** (Bivi, et al. 2016). When the sidechain is truncated, affinity for binding to the bone is reduced resulting in poorer mechanical outcomes. Using *in silico* prediction modeling, it has been postulated that groove on the surface of collagen may serve as a likely docking site due to the sufficient space for raloxifene's sidechain (**Figure 11E**).

The *in vitro* effects on hydration have been recapitulated in preclinical models. Initial work evaluating raloxifene following one year of treatment in skeletally mature female beagles resulted in significantly more total water in the cortical bone, assessed gravimetrically, compared to controls which positively correlated to

mechanical outcomes (**Figure 12A,B**) (Gallant, et al. 2014). In a separate study, skeletally mature female beagles treated with raloxifene for 6 months of had significantly higher bound water (+14%, p=0.05) and lower free water (-20%, p=0.05) compared to vehicle treated controls measured by UTE-MRI (**Figure 12C)** (Allen, et al. 2015b). It has been postulated that a pharmaceutical that acts independent of bone cells to exert positive increases in bone material properties would be a prime candidate to use in tandem with other therapies which act by decreasing resorption (bisphosphonates) or enhancing bone building (sclerostin antibody). Thus, when bound water was assessed in beagles treated with raloxifene, alendronate (bisphosphonate), or raloxifene and alendronate, it was observed that the greatest increase in this pool came from raloxifene alone, followed by raloxifene and alendronate, compared to controls (+23% and 18%) and no change from the alendronate group (**Figure 12D)** (Allen, et al. 2017). This suite of beagle studies using clinically relevant doses of raloxifene has since spurred several important pre-clinical studies looking at the efficacy of raloxifene across animal and disease models and in combination with other bone therapeutics (Eby, et al. 2021; Tastad, et al. 2021; K. M. Powell, et al. 2019; G. Wang, et al. 2021b).

Raloxifene's ability to improve bone in an estrogen-independent manner has motivated the synthesis of raloxifene analogs that can reduce and/or eliminate its affinity to ERα. This important modification would thereby mitigate hormone-related side effects making it suitable for a larger portion of the population (e.g., pediatric bone disorders). The first iteration of synthesized analog for bone, raloxifene Analog (RAL-A), replaces 6-hydroxy functionality in raloxifene with a methoxy substitute to create 6'-methoxyraloxifene and demonstrated significantly reduced (but not eliminated) ERα binding while demonstrating the hallmark improved toughness in a preclinical disease model (Katherine M. Powell, et al. 2020). Future synthesis work in needed to fully abolish ER binding.

6. Future Directions

Imaging advances have greatly enhanced our ability to study water across the bone hierarchy. This has led to a growing understanding of how bone water changes with age and disease and opened the possibility of therapeutically targeting water to improve its mechanical properties. Yet the cycle of research is such that new answers yield exponentially more questions. For example, can water transition between compartments? It has been proposed throughout the literature that tightly bound or structural water molecule is "released" to become

a loosely bound or free water molecule in the system (Kerch 2020). Others have even postulated that collagen-associated water can transition to structural water during mineralization of the osteoid (Nyman, et al. 2008) but this would depend upon docking site availability as there is already water associated with the mineral. Further, what regulates the amount of water that can be brought into the matrix? Is there molecular signaling at play or is it more of a passive process that is dictated by physical constituents? And how targetable are each of the compartments to modification and is to what degree can modifications in hydration offset loss of bone mass? These and of course countless other questions which when answered, will no doubt continue to change the way we think and approach enhancing bone health.

Acknowledgements: This work was supported by VA Merit Award (BX003025) from the U.S. Department of Veterans Affairs (Biomedical Laboratory Research and Development Service) to MRA, NSF Award (1952993) to JMW and MRA, NIH Award (R01AR072609) to JMW and the NIH award (T32DK120524) to RKS.

Figure Legends

Figure 1. ***Bone water is found in four functional compartments***. A) Free water is found within central canals and the lacunar-canalicular network. B) Water considered loosely bound is found at the interface of the collagen fibril and mineral crystals and can be associated with/loosely bound to collagen or mineral molecule. C) The tightly bound water fraction is bound to the collagen triple helix forming single and double water bridges, as cleft water within the grooves of the triple helix, and as water contributing to the interfacial monolayer. D) Structural water molecules are found incorporated around the mineral lattice of the carbonated apatite structures forming bridges of hydrogen bonds between ions within the apatite crystal.

Figure 2. ***The four functional water compartments play an integral role in governing bone's mechanical properties*****.** Theoretical force/displacement (A) and stress/strain (B) curves from a fully hydrated and dehydrated bone. A hydrated bone is a ductile material with high toughness and high work. When bone is dehydrated, the material becomes brittle, with high stiffness and modulus and significantly reduced post-yield behavior resulting in decreased toughness and work. While a dehydrated brittle bone can have higher strength (or higher peak/failure force) the lack of water in the system nullifies the plastic region and ductility in the tissue. The four water compartments differentially contribute to bone's mechanical properties. Loosely bound water governs post-yield behavior and increased loosely bound water results in increased toughness while increased tightly bound water decreases stiffness. Increased free water due to increased porosity and can negatively impact both stiffness and strength. Yet free water can also play a role in solute transport thus not all free water is indicative of cortical porosity. Little is known about the role of structural water and its role in governing whole bone mechanical properties. Because of its role in maintaining mineral structure and impacting assembly and aggregation, it likely has properties which govern both the elastic and plastic regions.

Figure 3. ***NMR water measures during dehydration highlight role in stabilizing matrix triglycerides.*** A) ^{1}H 1D NMR spectra of hydrated native bone (green) showing the distribution of free water (red), bound water (yellow) and lipid peaks. (B) ^{1}H 1D NMR spectra of H/D exchanged native bone and (C) dehydrated native bone. D) ^{1}H 1D Carr-Purcell-Meiboom-Gill NMR spectra (echo time = 2 ms) of hydrated native bone showing assigned spectral peaks of triglycerides. ^{1}H T_2 values from short component resonances (E) and long component

resonances (F) of the corresponding triglycerides shown in panel D depict several significant changes to the triglyceride structure under H/D exchange and dehydrated conditions compared to hydrated native bone. Adapted from Tiwari *et al*. and reprinted with permission (Tiwari, et al. 2020).

Figure 4. ***The amount of free water is regionally dependent.*** The left tibia from n=10 healthy volunteers (49 ± 15 yrs) underwent UTE-MRI at 3T and the cortices were divided into four quadrants (anterior, lateral, medial, posterior) for analysis. Pore water and total water (not shown) was significantly higher in the lateral region compared to the other three quadrants demonstrating regional dependence. $P<0.001$ via ANOVA followed by post-hoc analysis. Open-sourced figure from Zhao *et al*. (Zhao, et al. 2017).

Figure 5. ***UTE MRI-derived porosity index correlates to compositional and mechanical properties.*** A) Coronal (top) and transverse (bottom) views at the same slice location in the proximal cortical shaft of a human cadaveric femora specimen scanned on a clinical 3T scanner using a dual-echo UTE-MRI sequence. Echo 1 should ideally be acquired at the lowest possible TE to capture only bound water pools. The percent porosity index is computed by taking the intensity of Echo 2 divided by the intensity of Echo 1. B) Femora were subject to mechanical testing to mimic a sideways fall and porosity index (%) was significantly correlated with whole bone stiffness. Error clouds indicate 95% Confidence Intervals. Panel A and B adapted with permission from Jones *et al*. (B. C. Jones, et al. 2021). C) Porosity index was significantly correlated to bound water measured using near infrared spectroscopy imaging (NRISI). D) Example of NIRSI collagen, water, and porosity index colormaps for two cadavers. The first column is a 30-year-old female, and the second column is an 83-year-old female. Significant degradation of the endosteum can be seen in each scan of the older cadaver. Panel C and D adapted with permission from Hong *et al*. (Hong, et al. 2019).

Figure 6. ***3D UTE Cones MRI can detect bound, free and collagen water in vivo***. A) Generated proton density maps showing total water, bound water, pore/free and macromolecular (collagen) proton densities from two young volunteers (34 yrs, a2-a5 and 35 yrs, b2-b5) and two aged volunteers (75 yrs, c2-c5 and 76 yrs, d2-d5). B) Corresponding average proton densities from *in vivo* acquisitions (ten young healthy 34 ± 3 yrs and five aged women 78 ± 6 yrs). C) Scatter plot and linear regression analyses of the macromolecular proton density and μCT-derived cortical porosity. Analysis was performed on using *ex vivo* acquisitions from eight donor specimens

(63 ± 19 years old, 5 women, 3 men). Images adapted from Jerban *et al.* with permission (Saeed Jerban, et al. 2019b).

Figure 7. ***Raman collagen- and mineral- related water measures correlate with bone mechanical properties***. A) Average Raman intensity changes of bone during sequential dehydration in an oven for 48 hrs followed by ethanol treatment. There was a gradual decline in the Raman intensities of bone's OH-stretch band during sequential drying. Every spectral trace provided in this figure is the average of 90 spectra. Spectra are normalized with respect to the CH-stretch intensity that is representing the amount of protein in bone. R^2 pairwise correlations between mechanical properties (3-point bending) and Raman spectroscopic bone water biomarkers obtained from oven-dried bone samples. Significant correlations exist between collagen associated water (B) (I_{3220}/I_{2949}) o-d and toughness and (C) (I_{3220}/I_{2949}) o-d and post-yield toughness. Mineral associated water was significantly correlated (D) (I_{3584}/I_{2949}) o-d and maximum flexural strength, and (E) (I_{3584}/I_{2949}) o-d and the modulus. Reprinted with permission from Unal *et al*. (Unal and Akkus 2015).

Figure 8. ***Aging reduces bound water and tissue-level toughness***. A) Age-related effects in the amount of bound water measured via NMR and B) tissue-level toughness via nanoscratch test. Data shown are mean ± SD. n = 6. *p < 0.05. C) Bound water was significantly positively correlated with tissue-level toughness ($p<0.05$). Figures adapted from Wang *et al*. (X. Wang, et al. 2018).

Figure 9. ***Matrix hydration is differently impacted in low- vs. high turnover CKD.*** A) Pore water fraction at the femoral cortex measured via NMR was significantly higher in high turnover CKD and significantly lower in low turnover CKD compared to normal littermates. Bound water fraction was significantly lower in high turnover CKD and higher in low turnover CKD compared to normal littermates. All data presented as mean +/- standard deviation. * $p < 0.05$ compared to normal animals. B) Plasma PTH was positively correlated with pore water fraction ($r =0.81$) and C) negatively correlated with bound water fraction ($r = -0.70$). Figures adapted from Allen *et al*. (Allen, et al. 2015a).

Figure 10. ***Higher mineral and matrix-bound water in OIM mice is negatively correlated with stiffness and maximum load***. A) Hydrated OIM mouse cortical bone (humerii) had significantly higher total water content compared to wildtype (WT) measured using near-infrared (NIR) spectroscopy (*$p<0.05$). B) OIM had higher

mineral and matrix-bound water content relative to protein in lyophilized samples compared to WT (*p<0.05). C) Mineral and matrix-bound water relative to total protein was negatively correlated to stiffness (r= -0.44, p<0.05) and D) maximum load (r= -0.60, p<0.05). Figures from Shanas *et al*. adapted with permission (Shanas, et al. 2021).

Figure 11. ***Raloxifene interacts with collagen, collagen/mineral, but not mineral alone***. A) The structural features of RAL include a basic side chain and a benzothiophene core with a hydroxy in 6 and 4'. Detection and relative quantification of RAL in the supernatant after incubation (1, 4, 8 hrs; 50 μM concentration) without (control) and with 10 mg dog bone powder (B) or collagen (C) using solution state NMR. The amount of RAL in the supernatant was sig. reduced following incubation with both bone powder and collagen indicating the compound was retained in the bone and by collagen (and no longer in the solution). *p<0.05 by t-test vs. control. All graphs represent the integral of the peaks, bars are mean +/- standard deviation and each bar is the average of n=3 per group. D) RAL was incubated with bone powder, hydroxyapatite (HAP) or alone (control). HAP incubation did not elicit a decrease but rather resulted in an increase in the amount of RAL recovered in the supernatant while incubation with BP resulted in a 54.2% reduction in signal after 1 hour and 99% after 16 hours. Bars represent fold change relative to control. N=2. E) The basic side-chain appears to be a crucial structural requirement for bone matrix binding. Molecular modeling using SiteMap shows a collagen triple chain fiber molecular surface with putative binding sites/grooves for RAL indicated by small white spheres near the center (arrows). These grooves have sufficient space to accommodate RAL and are rich with acidic glutamate residues which is consistent with affinity for the basic side chain. Figures from Bivi *et al*. adapted with permission (Bivi, et al. 2016).

Figure 12. ***Raloxifene treatment in vivo increases cortical water*.** A) Water content measured gravimetrically was significantly higher (+5%) in bone samples from canines treated for 1 year with Raloxifene (RAL, 0.5 mg/kg/day, n=7) compared to vehicle treated canines (VEH, saline, 1 ml/kg/day, n=7). **p < 0.01 compared to VEH. B) Water content in canine bone treated for 1 year with RAL positively correlated with bone toughness measured via 4-point bending test. No relationship was observed in VEH treated controls. C) Raloxifene treatment leads to lower free water and higher bound water in cortical bone of skeletally mature female beagles following 6 months of RAL treatment (0.5 mg/kg/day, n=6) compared to VEH treatment (1 ml/kg/day, n=6). Water

was assessed using UTE-MRI and presented as % water fraction. *p=0.05 between groups using a one-tailed t test. D) Bound water measured via UTE-MRI at the proximal tibia of skeletally mature female beagles was significantly higher in RAL treated and RAL+alendronate (combo) treated animals relative to VEH. *p<0.05 when groups were pooled (6 month + 12 month, n=12) relative to VEH groups. Panel A and B (Gallant, et al. 2014) and D (Allen, et al. 2017) reprinted with permissions. Panel C adapted from Allen et al. (Allen, et al. 2015b).

References

[1] A.L. Boskey, P.G. Robey, The Composition of Bone, Primer on the Metabolic Bone Diseases and Disorders of Mineral Metabolism2018, pp. 84-92.
[2] R.A. Robinson, An electron-microscopic study of the crystalline inorganic component of bone and its relationship to the organic matrix, J Bone Joint Surg Am 34-A(2) (1952) 389-435; passim.
[3] W.F. Neuman, M.W. Neuman, The chemical dynamics of bone mineral, The chemical dynamics of bone mineral. (1958).
[4] J. Yan, A. Daga, R. Kumar, J.J. Mecholsky, Fracture toughness and work of fracture of hydrated, dehydrated, and ashed bovine bone, J Biomech 41(9) (2008) 1929-36 10.1016/j.jbiomech.2008.03.037.
[5] J.S. Nyman, A. Roy, X. Shen, R.L. Acuna, J.H. Tyler, X. Wang, The influence of water removal on the strength and toughness of cortical bone, J Biomech 39(5) (2006) 931-8 10.1016/j.jbiomech.2005.01.012.
[6] X. Wang, R. Hua, A. Ahsan, Q. Ni, Y. Huang, S. Gu, J.X. Jiang, Age-Related Deterioration of Bone Toughness Is Related to Diminishing Amount of Matrix Glycosaminoglycans (Gags), JBMR Plus 2(3) (2018) 164-173 10.1002/jbm4.10030.
[7] M.R. Allen, C.L. Newman, N. Chen, M. Granke, J.S. Nyman, S.M. Moe, Changes in skeletal collagen cross-links and matrix hydration in high- and low-turnover chronic kidney disease, Osteoporos Int 26(3) (2015a) 977-85 10.1007/s00198-014-2978-9.
[8] M.A. Gallant, D.M. Brown, M. Hammond, J.M. Wallace, J. Du, A.C. Deymier-Black, J.D. Almer, S.R. Stock, M.R. Allen, D.B. Burr, Bone cell-independent benefits of raloxifene on the skeleton: a novel mechanism for improving bone material properties, Bone 61 (2014) 191-200 10.1016/j.bone.2014.01.009.
[9] S.R. Elliott, R.A. Robinson, The water content of bone. I. The mass of water, inorganic crystals, organic matrix, and CO2 space components in a unit volume of the dog bone, J Bone Joint Surg Am 39-A(1) (1957) 167-88.
[10] M.A. Fernandez-Seara, S.L. Wehrli, M. Takahashi, F.W. Wehrli, Water content measured by proton-deuteron exchange NMR predicts bone mineral density and mechanical properties, J Bone Miner Res 19(2) (2004) 289-96 10.1359/JBMR.0301227.
[11] F.G. Evans, M. Lebow, Regional differences in some of the physical properties of the human femur, J Appl Physiol 3(9) (1951) 563-72 10.1152/jappl.1951.3.9.563.
[12] H. Yamada, F.G. Evans, Strength of biological materials, Williams & Wilkins, Baltimore,, 1970.
[13] E.D. Sedlin, C. Hirsch, Factors affecting the determination of the physical properties of femoral cortical bone, Acta Orthop Scand 37(1) (1966) 29-48 10.3109/17453676608989401.
[14] J.Y. Rho, G.M. Pharr, Effects of drying on the mechanical properties of bovine femur measured by nanoindentation, J Mater Sci Mater Med 10(8) (1999) 485-8 10.1023/a:1008901109705.
[15] W.T. Dempster, R.T. Liddicoat, Compact bone as a non-isotropic material, Am J Anat 91(3) (1952) 331-62 10.1002/aja.1000910302.
[16] F.G. Evans, Factors affecting the mechanical properties of bone, Bull N Y Acad Med 49(9) (1973) 751-64.
[17] W. Robinson, Free and bound water determinations by the heat of fusion of ice method, J Biol Chem (92) (1931) 699-709.
[18] M. Granke, M.D. Does, J.S. Nyman, The Role of Water Compartments in the Material Properties of Cortical Bone, Calcif Tissue Int 97(3) (2015a) 292-307 10.1007/s00223-015-9977-5.
[19] R. Biswas, W. Bae, E. Diaz, K. Masuda, C.B. Chung, G.M. Bydder, J. Du, Ultrashort echo time (UTE) imaging with bi-component analysis: bound and free water evaluation of bovine cortical bone subject to sequential drying, Bone 50(3) (2012) 749-55 10.1016/j.bone.2011.11.029.
[20] F.W. Wehrli, M.A. Fernandez-Seara, Nuclear magnetic resonance studies of bone water, Ann Biomed Eng 33(1) (2005) 79-86 10.1007/s10439-005-8965-8.
[21] C.S. Rajapakse, M. Bashoor-Zadeh, C. Li, W. Sun, A.C. Wright, F.W. Wehrli, Volumetric Cortical Bone Porosity Assessment with MR Imaging: Validation and Clinical Feasibility, Radiology 276(2) (2015) 526-35 10.1148/radiol.15141850.
[22] J. Liu, Z. Hou, Q.-H. Qin, D. Fu, S. Pan, Variation of Streaming Potentials with Time under Steady Fluid Pressure in Bone, Applied Sciences 9(18) (2019) 3726.
[23] D.A. Monteiro, N.S. Dole, J.L. Campos, S. Kaya, C.A. Schurman, C.D. Belair, T. Alliston, Fluid shear stress generates a unique signaling response by activating multiple TGFbeta family type I receptors in osteocytes, FASEB J 35(3) (2021) e21263 10.1096/fj.202001998R.
[24] E.R. Moore, H.S. Ryu, Y.X. Zhu, C.R. Jacobs, Adenylyl cyclases and TRPV4 mediate Ca(2+)/cAMP dynamics to enhance fluid flow-induced osteogenesis in osteocytes, J Mol Biochem 7 (2018) 48-59.
[25] A.E. Morrell, G.N. Brown, S.T. Robinson, R.L. Sattler, A.D. Baik, G. Zhen, X. Cao, L.F. Bonewald, W. Jin, L.C. Kam, X.E. Guo, Mechanically induced Ca(2+) oscillations in osteocytes release extracellular vesicles and enhance bone formation, Bone Res 6 (2018) 6 10.1038/s41413-018-0007-x.

[26] S. Wang, H. Suhaimi, M. Mabrouk, S. Georgiadou, J.P. Ward, D.B. Das, Effects of Scaffold Pore Morphologies on Glucose Transport Limitations in Hollow Fibre Membrane Bioreactor for Bone Tissue Engineering: Experiments and Numerical Modelling, Membranes (Basel) 11(4) (2021a) 10.3390/membranes11040257.
[27] L. Wang, Solute Transport in the Bone Lacunar-Canalicular System (LCS), Curr Osteoporos Rep 16(1) (2018) 32-41 10.1007/s11914-018-0414-3.
[28] S. Lees, A mixed packing model for bone collagen, Calcif Tissue Int 33(6) (1981) 591-602 10.1007/BF02409497.
[29] H.H. Ong, A.C. Wright, F.W. Wehrli, Deuterium nuclear magnetic resonance unambiguously quantifies pore and collagen-bound water in cortical bone, J Bone Miner Res 27(12) (2012) 2573-81 10.1002/jbmr.1709.
[30] H. Cao, J.L. Ackerman, M.I. Hrovat, L. Graham, M.J. Glimcher, Y. Wu, Quantitative bone matrix density measurement by water- and fat-suppressed proton projection MRI (WASPI) with polymer calibration phantoms, Magn Reson Med 60(6) (2008) 1433-43 10.1002/mrm.21771.
[31] F.-C. Wang, Y.-P. Zhao, Slip boundary conditions based on molecular kinetic theory: The critical shear stress and the energy dissipation at the liquid–solid interface, Soft Matter 7(18) (2011) 8628-8634 10.1039/C1SM05543G.
[32] J. Samuel, J.S. Park, J. Almer, X. Wang, Effect of water on nanomechanics of bone is different between tension and compression, J Mech Behav Biomed Mater 57 (2016a) 128-38 10.1016/j.jmbbm.2015.12.001.
[33] J.S. Nyman, L.E. Gorochow, R. Adam Horch, S. Uppuganti, A. Zein-Sabatto, M.K. Manhard, M.D. Does, Partial removal of pore and loosely bound water by low-energy drying decreases cortical bone toughness in young and old donors, J Mech Behav Biomed Mater 22 (2013) 136-45 10.1016/j.jmbbm.2012.08.013.
[34] P.A. Timmins, J.C. Wall, Bone water, Calcif Tissue Res 23(1) (1977) 1-5 10.1007/BF02012759.
[35] A.A. Marino, R.O. Becker, C.H. Bachman, Dielectric determination of bound water of bone, Phys Med Biol 12(3) (1967) 367-78 10.1088/0031-9155/12/3/309.
[36] S.M. Best, M.J. Duer, D.G. Reid, E.R. Wise, S. Zou, Towards a model of the mineral-organic interface in bone: NMR of the structure of synthetic glycosaminoglycan- and polyaspartate-calcium phosphate composites, Magn Reson Chem 46(4) (2008) 323-9 10.1002/mrc.2168.
[37] Y. Hashimoto, G.E. Lester, B. Caterson, M. Yamauchi, EDTA-insoluble, calcium-binding proteoglycan in bovine bone, Calcif Tissue Int 56(5) (1995) 398-402 10.1007/BF00301609.
[38] X. Wang, H. Xu, Y. Huang, S. Gu, J.X. Jiang, Coupling Effect of Water and Proteoglycans on the In Situ Toughness of Bone, J Bone Miner Res 31(5) (2016) 1026-9 10.1002/jbmr.2774.
[39] Y. Han, J. Gomez, R. Hua, P. Xiao, W. Gao, J.X. Jiang, X. Wang, Removal of glycosaminoglycans affects the in situ mechanical behavior of extrafibrillar matrix in bone, J Mech Behav Biomed Mater 123 (2021) 104766 10.1016/j.jmbbm.2021.104766.
[40] R. Hua, Q. Ni, T.D. Eliason, Y. Han, S. Gu, D.P. Nicolella, X. Wang, J.X. Jiang, Biglycan and chondroitin sulfate play pivotal roles in bone toughness via retaining bound water in bone mineral matrix, Matrix Biol 94 (2020) 95-109 10.1016/j.matbio.2020.09.002.
[41] Y. Henrotin, M. Mathy, C. Sanchez, C. Lambert, Chondroitin sulfate in the treatment of osteoarthritis: from in vitro studies to clinical recommendations, Ther Adv Musculoskelet Dis 2(6) (2010) 335-48 10.1177/1759720X10383076.
[42] J.S. Nyman, S. Uppuganti, M. Unal, C.J. Leverant, S. Adabala, M. Granke, P. Voziyan, M.D. Does, Manipulating the Amount and Structure of the Organic Matrix Affects the Water Compartments of Human Cortical Bone, JBMR Plus 3(6) (2019) e10135 10.1002/jbm4.10135.
[43] E.E. Wilson, A. Awonusi, M.D. Morris, D.H. Kohn, M.M. Tecklenburg, L.W. Beck, Highly ordered interstitial water observed in bone by nuclear magnetic resonance, J Bone Miner Res 20(4) (2005) 625-34 10.1359/JBMR.041217.
[44] M. Unal, O. Akkus, Raman spectral classification of mineral- and collagen-bound water's associations to elastic and post-yield mechanical properties of cortical bone, Bone 81 (2015) 315-326 10.1016/j.bone.2015.07.024.
[45] L. Eberhardsteiner, C. Hellmich, S. Scheiner, Layered water in crystal interfaces as source for bone viscoelasticity: arguments from a multiscale approach, Comput Methods Biomech Biomed Engin 17(1) (2014) 48-63 10.1080/10255842.2012.670227.
[46] Y. Wang, S. Von Euw, F.M. Fernandes, S. Cassaignon, M. Selmane, G. Laurent, G. Pehau-Arnaudet, C. Coelho, L. Bonhomme-Coury, M.M. Giraud-Guille, F. Babonneau, T. Azais, N. Nassif, Water-mediated structuring of bone apatite, Nat Mater 12(12) (2013) 1144-53 10.1038/nmat3787.
[47] A. Faingold, S.R. Cohen, R. Shahar, S. Weiner, L. Rapoport, H.D. Wagner, The effect of hydration on mechanical anisotropy, topography and fibril organization of the osteonal lamellae, J Biomech 47(2) (2014) 367-72 10.1016/j.jbiomech.2013.11.022.
[48] S. Von Euw, T.-H.-C. Chan-Chang, C. Paquis, B. Haye, G. Pehau-Arnaudet, F. Babonneau, T. Azaïs, N. Nassif, Organization of Bone Mineral: The Role of Mineral–Water Interactions, Geosciences 8(12) (2018) 466.
[49] A.M. Drouet C, Rollin-Martinet S, Vandecandelaere N, Grossin D, Rossignol F, Nanocrystalline apatites: The fundamental role of water, American Mineralogist 103(4) (2018) 550-564 https://doi.org/10.2138/am-2018-6415.
[50] V. Vaissier Welborn, Environment-controlled water adsorption at hydroxyapatite/collagen interfaces, Physical Chemistry Chemical Physics 23(25) (2021) 13789-13796 10.1039/D1CP01028J.

[51] P. Ivanchenko, J.M. Delgado-Lopez, M. Iafisco, J. Gomez-Morales, A. Tampieri, G. Martra, Y. Sakhno, On the surface effects of citrates on nano-apatites: evidence of a decreased hydrophilicity, Sci Rep 7(1) (2017) 8901 10.1038/s41598-017-09376-x.
[52] P.L. Privalov, [State and role of water in biological systems], Biofizika 3(6) (1958) 738-43.
[53] A. Masic, L. Bertinetti, R. Schuetz, S.W. Chang, T.H. Metzger, M.J. Buehler, P. Fratzl, Osmotic pressure induced tensile forces in tendon collagen, Nat Commun 6 (2015) 5942 10.1038/ncomms6942.
[54] G.D. Fullerton, M.R. Amurao, Evidence that collagen and tendon have monolayer water coverage in the native state, Cell Biol Int 30(1) (2006) 56-65 10.1016/j.cellbi.2005.09.008.
[55] G.D. Fullerton, E. Nes, M. Amurao, A. Rahal, L. Krasnosselskaia, I. Cameron, An NMR method to characterize multiple water compartments on mammalian collagen, Cell Biol Int 30(1) (2006) 66-73 10.1016/j.cellbi.2005.09.009.
[56] H. Trebacz, K. Wojtowicz, Thermal stabilization of collagen molecules in bone tissue, Int J Biol Macromol 37(5) (2005) 257-62 10.1016/j.ijbiomac.2005.04.007.
[57] C.H. Yoder, J.D. Pasteris, K.N. Worcester, D.V. Schermerhorn, Structural water in carbonated hydroxylapatite and fluorapatite: confirmation by solid state (2)H NMR, Calcif Tissue Int 90(1) (2012) 60-7 10.1007/s00223-011-9542-9.
[58] E. Davies, K.H. Muller, W.C. Wong, C.J. Pickard, D.G. Reid, J.N. Skepper, M.J. Duer, Citrate bridges between mineral platelets in bone, Proc Natl Acad Sci U S A 111(14) (2014) E1354-63 10.1073/pnas.1315080111.
[59] B. Alexander, T.L. Daulton, G.M. Genin, J. Lipner, J.D. Pasteris, B. Wopenka, S. Thomopoulos, The nanometre-scale physiology of bone: steric modelling and scanning transmission electron microscopy of collagen-mineral structure, J R Soc Interface 9(73) (2012) 1774-86 10.1098/rsif.2011.0880.
[60] E.A. McNally, H.P. Schwarcz, G.A. Botton, A.L. Arsenault, A model for the ultrastructure of bone based on electron microscopy of ion-milled sections, PLoS One 7(1) (2012) e29258 10.1371/journal.pone.0029258.
[61] N. Reznikov, M. Bilton, L. Lari, M.M. Stevens, R. Kroger, Fractal-like hierarchical organization of bone begins at the nanoscale, Science 360(6388) (2018) 10.1126/science.aao2189.
[62] M. Duer, A. Veis, Bone mineralization: Water brings order, Nat Mater 12(12) (2013) 1081-2 10.1038/nmat3822.
[63] M. Mahesh, The Essential Physics of Medical Imaging, Third Edition, Med Phys 40(7) (2013) 10.1118/1.4811156.
[64] J.A. Kanis, Diagnosis of osteoporosis and assessment of fracture risk, Lancet 359(9321) (2002) 1929-36 10.1016/S0140-6736(02)08761-5.
[65] C.J. Hernandez, M.C. van der Meulen, Understanding Bone Strength Is Not Enough, J Bone Miner Res 32(6) (2017) 1157-1162 10.1002/jbmr.3078.
[66] D. Marshall, O. Johnell, H. Wedel, Meta-analysis of how well measures of bone mineral density predict occurrence of osteoporotic fractures, BMJ 312(7041) (1996) 1254-9 10.1136/bmj.312.7041.1254.
[67] F.A. Tremollieres, J.M. Pouilles, N. Drewniak, J. Laparra, C.A. Ribot, P. Dargent-Molina, Fracture risk prediction using BMD and clinical risk factors in early postmenopausal women: sensitivity of the WHO FRAX tool, J Bone Miner Res 25(5) (2010) 1002-9 10.1002/jbmr.12.
[68] O.R. Boughton, S. Ma, X. Cai, L. Yan, L. Peralta, P. Laugier, J. Marrow, F. Giuliani, U. Hansen, R.L. Abel, Q. Grimal, J.P. Cobb, Computed tomography porosity and spherical indentation for determining cortical bone millimetre-scale mechanical properties, Sci Rep 9(1) (2019) 7416 10.1038/s41598-019-43686-6.
[69] E.C. Lin, Radiation risk from medical imaging, Mayo Clin Proc 85(12) (2010) 1142-6; quiz 1146 10.4065/mcp.2010.0260.
[70] K. Laperre, M. Depypere, N. van Gastel, S. Torrekens, K. Moermans, R. Bogaerts, F. Maes, G. Carmeliet, Development of micro-CT protocols for in vivo follow-up of mouse bone architecture without major radiation side effects, Bone 49(4) (2011) 613-22 10.1016/j.bone.2011.06.031.
[71] H.J. Williams, A.M. Davies, The effect of X-rays on bone: a pictorial review, European Radiology 16(3) (2006) 619-633 10.1007/s00330-005-0010-7.
[72] P. Choksi, K.J. Jepsen, G.A. Clines, The challenges of diagnosing osteoporosis and the limitations of currently available tools, Clin Diabetes Endocrinol 4 (2018) 12 10.1186/s40842-018-0062-7.
[73] K.H. Mroue, Y. Nishiyama, M. Kumar Pandey, B. Gong, E. McNerny, D.H. Kohn, M.D. Morris, A. Ramamoorthy, Proton-Detected Solid-State NMR Spectroscopy of Bone with Ultrafast Magic Angle Spinning, Sci Rep 5 (2015) 11991 10.1038/srep11991.
[74] S. Jerban, Y. Ma, Z. Wei, H. Jang, E.Y. Chang, J. Du, Quantitative Magnetic Resonance Imaging of Cortical and Trabecular Bone, Semin Musculoskelet Radiol 24(04) (2020a) 386-401.
[75] C. Singh, R.K. Rai, N. Sinha, Experimental aspect of solid-state nuclear magnetic resonance studies of biomaterials such as bones, Solid State Nucl Magn Reson 54 (2013) 18-25 10.1016/j.ssnmr.2013.05.003.
[76] D.T. Murray, N. Das, T.A. Cross, Solid state NMR strategy for characterizing native membrane protein structures, Acc Chem Res 46(9) (2013) 2172-81 10.1021/ar3003442.
[77] C. Singh, R.K. Rai, F. Aussenac, N. Sinha, Direct Evidence of Imino Acid-Aromatic Interactions in Native Collagen Protein by DNP-Enhanced Solid-State NMR Spectroscopy, J Phys Chem Lett 5(22) (2014) 4044-8 10.1021/jz502081j.
[78] P. Fantazzini, R.J. Brown, G.C. Borgia, Bone tissue and porous media: common features and differences studied by NMR relaxation, Magn Reson Imaging 21(3-4) (2003) 227-34 10.1016/s0730-725x(03)00129-2.

[79] P. Fantazzini, V. Bortolotti, R.J.S. Brown, M. Camaiti, C. Garavaglia, R. Viola, G. Giavaresi, Two 1H-nuclear magnetic resonance methods to measure internal porosity of bone trabeculae: By solid–liquid signal separation and by longitudinal relaxation, Journal of Applied Physics 95(1) (2004) 339-343 10.1063/1.1630374.
[80] S.P. Brown, Applications of high-resolution 1H solid-state NMR, Solid State Nucl Magn Reson 41 (2012) 1-27 10.1016/j.ssnmr.2011.11.006.
[81] P. Hodgkinson, S. Wimperis, Solid-state NMR spectroscopy, Phys Chem Chem Phys 11(32) (2009) 6875 10.1039/b914008p.
[82] F. Casciani, Identification of hydrate water in enamel, dentine, cementum and bone, in: R.S. Fearnhead, MV (Ed.), Tooth Enamel II: its composition, properties and fundamental structure, John Wright & Sons, Ltd, Bristol, 1971, pp. 14-23.
[83] R.K. Rai, N. Sinha, Dehydration-Induced Structural Changes in the Collagen–Hydroxyapatite Interface in Bone by High-Resolution Solid-State NMR Spectroscopy, The Journal of Physical Chemistry C 115(29) (2011) 14219-14227 10.1021/jp2025768.
[84] O. Nikel, D. Laurencin, C. Bonhomme, G.E. Sroga, S. Besdo, A. Lorenz, D. Vashishth, Solid state NMR investigation of intact human bone quality: balancing issues and insight into the structure at the organic-mineral interface, J Phys Chem C Nanomater Interfaces 116(10) (2012) 6320-6331 10.1021/jp2125312.
[85] R.A. Horch, J.S. Nyman, D.F. Gochberg, R.D. Dortch, M.D. Does, Characterization of 1H NMR signal in human cortical bone for magnetic resonance imaging, Magn Reson Med 64(3) (2010) 680-7 10.1002/mrm.22459.
[86] R.K. Rai, T. Barbhuyan, C. Singh, M. Mittal, M.P. Khan, N. Sinha, N. Chattopadhyay, Total water, phosphorus relaxation and inter-atomic organic to inorganic interface are new determinants of trabecular bone integrity, PLoS One 8(12) (2013) e83478 10.1371/journal.pone.0083478.
[87] R.A. Horch, D.F. Gochberg, J.S. Nyman, M.D. Does, Non-invasive predictors of human cortical bone mechanical properties: T(2)-discriminated H NMR compared with high resolution X-ray, PLoS One 6(1) (2011) e16359 10.1371/journal.pone.0016359.
[88] K.H. Mroue, J. Xu, P. Zhu, M.D. Morris, A. Ramamoorthy, Selective detection and complete identification of triglycerides in cortical bone by high-resolution (1)H MAS NMR spectroscopy, Phys Chem Chem Phys 18(28) (2016) 18687-91 10.1039/c6cp03506j.
[89] N. Tiwari, R. Rai, N. Sinha, Water-lipid interactions in native bone by high-resolution solid-state NMR spectroscopy, Solid State Nucl Magn Reson 107 (2020) 101666 10.1016/j.ssnmr.2020.101666.
[90] R.K. Rai, C. Singh, N. Sinha, Predominant role of water in native collagen assembly inside the bone matrix, J Phys Chem B 119(1) (2015) 201-11 10.1021/jp511288g.
[91] K.H. Mroue, N. MacKinnon, J. Xu, P. Zhu, E. McNerny, D.H. Kohn, M.D. Morris, A. Ramamoorthy, High-resolution structural insights into bone: a solid-state NMR relaxation study utilizing paramagnetic doping, The journal of physical chemistry. B 116(38) (2012) 11656-11661 10.1021/jp307935g.
[92] D. Reichert, O. Pascui, E.R. deAzevedo, T.J. Bonagamba, K. Arnold, D. Huster, A solid-state NMR study of the fast and slow dynamics of collagen fibrils at varying hydration levels, Magn Reson Chem 42(2) (2004) 276-84 10.1002/mrc.1334.
[93] P. Zhu, J. Xu, N. Sahar, M.D. Morris, D.H. Kohn, A. Ramamoorthy, Time-resolved dehydration-induced structural changes in an intact bovine cortical bone revealed by solid-state NMR spectroscopy, J Am Chem Soc 131(47) (2009a) 17064-5 10.1021/ja9081028.
[94] E.E. Wilson, A. Awonusi, M.D. Morris, D.H. Kohn, M.M. Tecklenburg, L.W. Beck, Three structural roles for water in bone observed by solid-state NMR, Biophys J 90(10) (2006) 3722-31 10.1529/biophysj.105.070243.
[95] A. Vyalikh, C. Elschner, M.C. Schulz, R. Mai, U. Scheler, Early Stages of Biomineral Formation—A Solid-State NMR Investigation of the Mandibles of Minipigs, Magnetochemistry 3(4) (2017) 39.
[96] S. Mastrogiacomo, W. Dou, J.A. Jansen, X.F. Walboomers, Magnetic Resonance Imaging of Hard Tissues and Hard Tissue Engineered Bio-substitutes, Mol Imaging Biol 21(6) (2019) 1003-1019 10.1007/s11307-019-01345-2.
[97] J. Damilakis, J.E. Adams, G. Guglielmi, T.M. Link, Radiation exposure in X-ray-based imaging techniques used in osteoporosis, Eur Radiol 20(11) (2010) 2707-14 10.1007/s00330-010-1845-0.
[98] J.S. Nyman, Q. Ni, D.P. Nicolella, X. Wang, Measurements of mobile and bound water by nuclear magnetic resonance correlate with mechanical properties of bone, Bone 42(1) (2008) 193-9 10.1016/j.bone.2007.09.049.
[99] M.D. Robson, G.M. Bydder, Clinical ultrashort echo time imaging of bone and other connective tissues, NMR Biomed 19(7) (2006) 765-80 10.1002/nbm.1100.
[100] P. Siriwanarangsun, S. Statum, R. Biswas, W.C. Bae, C.B. Chung, Ultrashort time to echo magnetic resonance techniques for the musculoskeletal system, Quant Imaging Med Surg 6(6) (2016) 731-743 10.21037/qims.2016.12.06.
[101] S. Hafner, Fast imaging in liquids and solids with the Back-projection Low Angle ShoT (BLAST) technique, Magn Reson Imaging 12(7) (1994) 1047-51 10.1016/0730-725x(94)91236-p.
[102] D.P. Madio, I.J. Lowe, Ultra-fast imaging using low flip angles and FIDs, Magn Reson Med 34(4) (1995) 525-9 10.1002/mrm.1910340407.
[103] M. Weiger, K.P. Pruessmann, F. Hennel, MRI with zero echo time: hard versus sweep pulse excitation, Magn Reson Med 66(2) (2011) 379-89 10.1002/mrm.22799.

[104] D. Idiyatullin, C. Corum, J.Y. Park, M. Garwood, Fast and quiet MRI using a swept radiofrequency, J Magn Reson 181(2) (2006) 342-9 10.1016/j.jmr.2006.05.014.
[105] Y.J. Ma, S. Jerban, H. Jang, D. Chang, E.Y. Chang, J. Du, Quantitative Ultrashort Echo Time (UTE) Magnetic Resonance Imaging of Bone: An Update, Front Endocrinol (Lausanne) 11 (2020a) 567417 10.3389/fendo.2020.567417.
[106] W.C. Bae, P.C. Chen, C.B. Chung, K. Masuda, D. D'Lima, J. Du, Quantitative ultrashort echo time (UTE) MRI of human cortical bone: correlation with porosity and biomechanical properties, J Bone Miner Res 27(4) (2012a) 848-57 10.1002/jbmr.1535.
[107] X. Zhao, H.K. Song, A.C. Seifert, C. Li, F.W. Wehrli, Feasibility of assessing bone matrix and mineral properties in vivo by combined solid-state 1H and 31P MRI, PLOS ONE 12(3) (2017) e0173995 10.1371/journal.pone.0173995.
[108] M.K. Manhard, S. Uppuganti, M. Granke, D.F. Gochberg, J.S. Nyman, M.D. Does, MRI-derived bound and pore water concentrations as predictors of fracture resistance, Bone 87 (2016) 1-10 https://doi.org/10.1016/j.bone.2016.03.007.
[109] W.C. Bae, P.C. Chen, C.B. Chung, K. Masuda, D. D'Lima, J. Du, Quantitative ultrashort echo time (UTE) MRI of human cortical bone: correlation with porosity and biomechanical properties, Journal of bone and mineral research : the official journal of the American Society for Bone and Mineral Research 27(4) (2012b) 848-857 10.1002/jbmr.1535.
[110] S. Jerban, Y. Ma, J.H. Wong, A. Nazaran, A. Searleman, L. Wan, J. Williams, J. Du, E.Y. Chang, Ultrashort echo time magnetic resonance imaging (UTE-MRI) of cortical bone correlates well with histomorphometric assessment of bone microstructure, Bone 123 (2019a) 8-17 10.1016/j.bone.2019.03.013.
[111] A.C. Seifert, S.L. Wehrli, F.W. Wehrli, Bi-component T2 * analysis of bound and pore bone water fractions fails at high field strengths, NMR in biomedicine 28(7) (2015) 861-872 10.1002/nbm.3305.
[112] S. Li, L. Ma, E.Y. Chang, H. Shao, J. Chen, C.B. Chung, G.M. Bydder, J. Du, Effects of inversion time on inversion recovery prepared ultrashort echo time (IR-UTE) imaging of bound and pore water in cortical bone, NMR in biomedicine 28(1) (2015) 70-78 10.1002/nbm.3228.
[113] X. Lu, S. Jerban, L. Wan, Y. Ma, H. Jang, N. Le, W. Yang, E.Y. Chang, J. Du, Three-dimensional ultrashort echo time imaging with tricomponent analysis for human cortical bone, Magnetic resonance in medicine 82(1) (2019) 348-355 10.1002/mrm.27718.
[114] S. Jerban, X. Lu, E.W. Dorthe, S. Alenezi, Y. Ma, L. Kakos, H. Jang, R.L. Sah, E.Y. Chang, D. D'Lima, J. Du, Correlations of cortical bone microstructural and mechanical properties with water proton fractions obtained from ultrashort echo time (UTE) MRI tricomponent T2* model, NMR in biomedicine 33(3) (2020b) e4233-e4233 10.1002/nbm.4233.
[115] R.A. Horch, D.F. Gochberg, J.S. Nyman, M.D. Does, Clinically compatible MRI strategies for discriminating bound and pore water in cortical bone, Magnetic resonance in medicine 68(6) (2012) 1774-1784 10.1002/mrm.24186.
[116] M.K. Manhard, R.A. Horch, D.F. Gochberg, J.S. Nyman, M.D. Does, In Vivo Quantitative MR Imaging of Bound and Pore Water in Cortical Bone, Radiology 277(1) (2015) 221-229 10.1148/radiol.2015140336.
[117] A.C. Seifert, F.W. Wehrli, Solid-State Quantitative (1)H and (31)P MRI of Cortical Bone in Humans, Current osteoporosis reports 14(3) (2016) 77-86 10.1007/s11914-016-0307-2.
[118] E.Y. Chang, J. Du, C.B. Chung, UTE imaging in the musculoskeletal system, Journal of magnetic resonance imaging : JMRI 41(4) (2015a) 870-883 10.1002/jmri.24713.
[119] J. Du, M. Carl, M. Bydder, A. Takahashi, C.B. Chung, G.M. Bydder, Qualitative and quantitative ultrashort echo time (UTE) imaging of cortical bone, Journal of Magnetic Resonance 207(2) (2010) 304-311 https://doi.org/10.1016/j.jmr.2010.09.013.
[120] Y.-J. Ma, S. Jerban, H. Jang, D. Chang, E.Y. Chang, J. Du, Quantitative Ultrashort Echo Time (UTE) Magnetic Resonance Imaging of Bone: An Update, Frontiers in endocrinology 11 (2020b) 567417-567417 10.3389/fendo.2020.567417.
[121] B.C. Jones, S. Jia, H. Lee, A. Feng, S.S. Shetye, A. Batzdorf, N. Shapira, P.B. Noel, N. Pleshko, C.S. Rajapakse, MRI-derived porosity index is associated with whole-bone stiffness and mineral density in human cadaveric femora, Bone 143 (2021) 115774 10.1016/j.bone.2020.115774.
[122] E.Y. Chang, W.C. Bae, H. Shao, R. Biswas, S. Li, J. Chen, S. Patil, R. Healey, D.D. D'Lima, C.B. Chung, J. Du, Ultrashort echo time magnetization transfer (UTE-MT) imaging of cortical bone, NMR Biomed 28(7) (2015b) 873-80 10.1002/nbm.3316.
[123] A.L. Hong, M. Ispiryan, M.V. Padalkar, B.C. Jones, A.S. Batzdorf, S.S. Shetye, N. Pleshko, C.S. Rajapakse, MRI-derived bone porosity index correlates to bone composition and mechanical stiffness, Bone Rep 11 (2019) 100213 10.1016/j.bonr.2019.100213.
[124] M. Weiger, K.P. Pruessmann, A.-K. Bracher, S. Köhler, V. Lehmann, U. Wolfram, F. Hennel, V. Rasche, High-resolution ZTE imaging of human teeth, NMR in Biomedicine 25(10) (2012) 1144-1151 https://doi.org/10.1002/nbm.2783.
[125] M. Marcon, D. Keller, M.C. Wurnig, M. Weiger, D. Kenkel, C. Eberhardt, D. Eberli, A. Boss, Separation of collagen-bound and porous bone-water longitudinal relaxation in mice using a segmented inversion recovery zero-echo-time sequence, Magnetic Resonance in Medicine 77(5) (2017) 1909-1915 https://doi.org/10.1002/mrm.26277.
[126] Y.-J. Ma, E.Y. Chang, M. Carl, J. Du, Quantitative magnetization transfer ultrashort echo time imaging using a time-efficient 3D multispoke Cones sequence, Magnetic resonance in medicine 79(2) (2018) 692-700 10.1002/mrm.26716.

[127] Y.-J. Ma, H. Shao, J. Du, E.Y. Chang, Ultrashort echo time magnetization transfer (UTE-MT) imaging and modeling: magic angle independent biomarkers of tissue properties, NMR in biomedicine 29(11) (2016) 1546-1552 10.1002/nbm.3609.
[128] S. Jerban, Y. Ma, L. Li, H. Jang, L. Wan, T. Guo, A. Searleman, E.Y. Chang, J. Du, Volumetric mapping of bound and pore water as well as collagen protons in cortical bone using 3D ultrashort echo time cones MR imaging techniques, Bone 127 (2019b) 120-128 10.1016/j.bone.2019.05.038.
[129] R.R. Jones, D.C. Hooper, L. Zhang, D. Wolverson, V.K. Valev, Raman Techniques: Fundamentals and Frontiers, Nanoscale Research Letters 14(1) (2019) 231 10.1186/s11671-019-3039-2.
[130] M. Bergholt, A. Serio, M. Albro, Raman Spectroscopy: Guiding Light for the Extracellular Matrix, Frontiers in Bioengineering and Biotechnology 7(303) (2019) 10.3389/fbioe.2019.00303.
[131] M.D. Morris, G.S. Mandair, Raman assessment of bone quality, Clin Orthop Relat Res 469(8) (2011) 2160-2169 10.1007/s11999-010-1692-y.
[132] A.J. Makowski, M. Granke, O.D. Ayala, S. Uppuganti, A. Mahadevan-Jansen, J.S. Nyman, Applying Full Spectrum Analysis to a Raman Spectroscopic Assessment of Fracture Toughness of Human Cortical Bone, Appl Spectrosc 71(10) (2017) 2385-2394 10.1177/0003702817718149.
[133] G. Penel, C. Delfosse, M. Descamps, G. Leroy, Composition of bone and apatitic biomaterials as revealed by intravital Raman microspectroscopy, Bone 36(5) (2005) 893-901 https://doi.org/10.1016/j.bone.2005.02.012.
[134] E. Donnelly, A.L. Boskey, S.P. Baker, M.C.H. van der Meulen, Effects of tissue age on bone tissue material composition and nanomechanical properties in the rat cortex, J Biomed Mater Res A 92(3) (2010) 1048-1056 10.1002/jbm.a.32442.
[135] M. Unal, S. Yang, O. Akkus, Molecular spectroscopic identification of the water compartments in bone, Bone 67 (2014) 228-36 10.1016/j.bone.2014.07.021.
[136] G. Chang, S. Boone, D. Martel, C.S. Rajapakse, R.S. Hallyburton, M. Valko, S. Honig, R.R. Regatte, MRI assessment of bone structure and microarchitecture, Journal of magnetic resonance imaging : JMRI 46(2) (2017) 323-337 10.1002/jmri.25647.
[137] C.S. Rajapakse, M.V. Padalkar, H.J. Yang, M. Ispiryan, N. Pleshko, Non-destructive NIR spectral imaging assessment of bone water: Comparison to MRI measurements, Bone 103 (2017) 116-124 10.1016/j.bone.2017.06.015.
[138] R. Ailavajhala, J. Oswald, C.S. Rajapakse, N. Pleshko, Environmentally-Controlled Near Infrared Spectroscopic Imaging of Bone Water, Scientific Reports 9(1) (2019) 10199 10.1038/s41598-019-45897-3.
[139] J. Xia, J. Yao, L.V. Wang, Photoacoustic tomography: principles and advances, Electromagn Waves (Camb) 147 (2014) 1-22 10.2528/pier14032303.
[140] P. Beard, Biomedical photoacoustic imaging, Interface Focus 1(4) (2011) 602-631 doi:10.1098/rsfs.2011.0028.
[141] E.Y. Park, D. Lee, C. Lee, C. Kim, Non-Ionizing Label-Free Photoacoustic Imaging of Bones, IEEE Access 8 (2020) 160915-160920 10.1109/ACCESS.2020.3020559.
[142] Z. Xu, C. Li, L.V. Wang, Photoacoustic tomography of water in phantoms and tissue, J Biomed Opt 15(3) (2010) 036019-036019 10.1117/1.3443793.
[143] B. Lashkari, A. Mandelis, Coregistered photoacoustic and ultrasonic signatures of early bone density variations, J Biomed Opt 19(3) (2014) 036015.
[144] T. Feng, J.E. Perosky, K.M. Kozloff, G. Xu, Q. Cheng, S. Du, J. Yuan, C.X. Deng, X. Wang, Characterization of bone microstructure using photoacoustic spectrum analysis, Opt Express 23(19) (2015) 25217-25224 10.1364/OE.23.025217.
[145] T. Feng, Y. Zhu, R. Morris, K.M. Kozloff, X. Wang, Functional Photoacoustic and Ultrasonic Assessment of Osteoporosis: A Clinical Feasibility Study, BMEF 2020 (2020) 1081540 10.34133/2020/1081540.
[146] T. Feng, Y. Ge, Y. Xie, W. Xie, C. Liu, L. Li, D. Ta, Q. Jiang, Q. Cheng, Detection of collagen by multi-wavelength photoacoustic analysis as a biomarker for bone health assessment, Photoacoustics 24 (2021) 100296 https://doi.org/10.1016/j.pacs.2021.100296.
[147] R.L. Sheer, R.L. Barron, L. Sudharshan, M.K. Pasquale, Validated prediction of imminent risk of fracture for older adults, Am J Manag Care 26(3) (2020) e91-e97 10.37765/ajmc.2020.42641.
[148] K.J. Koester, H.D. Barth, R.O. Ritchie, Effect of aging on the transverse toughness of human cortical bone: evaluation by R-curves, J Mech Behav Biomed Mater 4(7) (2011) 1504-13 10.1016/j.jmbbm.2011.05.020.
[149] O.L. Katsamenis, T. Jenkins, P.J. Thurner, Toughness and damage susceptibility in human cortical bone is proportional to mechanical inhomogeneity at the osteonal-level, Bone 76 (2015) 158-68 10.1016/j.bone.2015.03.020.
[150] D.B. Burr, C.H. Turner, CHAPTER 26 - Biomechanical Measurements in Age-Related Bone Loss, in: C.J. Rosen, J. Glowacki, J.P. Bilezikian (Eds.), The Aging Skeleton, Academic Press, San Diego, 1999, pp. 301-311.
[151] S.L. Hui, C.W. Slemenda, C.C. Johnston, Jr., Age and bone mass as predictors of fracture in a prospective study, J Clin Invest 81(6) (1988) 1804-9 10.1172/jci113523.
[152] J.A. Kanis, O. Johnell, A. Oden, A. Dawson, C. De Laet, B. Jonsson, Ten year probabilities of osteoporotic fractures according to BMD and diagnostic thresholds, Osteoporos Int 12(12) (2001) 989-95 10.1007/s001980170006.

[153] S. Jerban, Y. Ma, H. Jang, B. Namiranian, N. Le, H. Shirazian, M.E. Murphy, J. Du, E.Y. Chang, Water proton density in human cortical bone obtained from ultrashort echo time (UTE) MRI predicts bone microstructural properties, Magn Reson Imaging 67 (2020c) 85-89 10.1016/j.mri.2020.01.004.
[154] A. Akbari, S. Abbasi-Rad, H.S. Rad, T1 correlates age: A short-TE MR relaxometry study in vivo on human cortical bone free water at 1.5T, Bone 83 (2016) 17-22 10.1016/j.bone.2015.10.006.
[155] P. Zhu, J. Xu, N. Sahar, M.D. Morris, D.H. Kohn, A. Ramamoorthy, Time-Resolved Dehydration-Induced Structural Changes in an Intact Bovine Cortical Bone Revealed by Solid-State NMR Spectroscopy, Journal of the American Chemical Society 131(47) (2009b) 17064-17065 10.1021/ja9081028.
[156] J. Samuel, J.-S. Park, J. Almer, X. Wang, Effect of water on nanomechanics of bone is different between tension and compression, Journal of the mechanical behavior of biomedical materials 57 (2016b) 128-138 10.1016/j.jmbbm.2015.12.001.
[157] M. Granke, A.J. Makowski, S. Uppuganti, M.D. Does, J.S. Nyman, Identifying Novel Clinical Surrogates to Assess Human Bone Fracture Toughness, J Bone Miner Res 30(7) (2015b) 1290-300 10.1002/jbmr.2452.
[158] A. Creecy, S. Uppuganti, M.R. Girard, S.G. Schlunk, C. Amah, M. Granke, M. Unal, M.D. Does, J.S. Nyman, The age-related decrease in material properties of BALB/c mouse long bones involves alterations to the extracellular matrix, Bone 130 (2020) 115126 10.1016/j.bone.2019.115126.
[159] S. Uppuganti, M. Granke, A.J. Makowski, M.D. Does, J.S. Nyman, Age-related changes in the fracture resistance of male Fischer F344 rat bone, Bone 83 (2016) 220-232 10.1016/j.bone.2015.11.009.
[160] M.G. Bridelli, S. Chiaramaria, R. Bedotti, Fourier transform infrared conformational investigation of type I collagen aged by in vitro induced dehydration and non-enzymatic glycation treatments, Journal of Biological Research 90(1) (2017) http://dx.doi.org/10.4081/jbr.2017.6254.
[161] E. Jazini, A.D. Sharan, L.J. Morse, J.P. Dyke, E.B. Aronowitz, L.K. Chen, S.Y. Tang, Alterations in T2 relaxation magnetic resonance imaging of the ovine intervertebral disc due to nonenzymatic glycation, Spine (Phila Pa 1976) 37(4) (2012) E209-15 10.1097/BRS.0b013e31822ce81f.
[162] J. Kopp, M. Bonnet, J.P. Renou, Effect of collagen crosslinking on collagen-water interactions (a DSC investigation), Matrix 9(6) (1989) 443-50 10.1016/s0934-8832(11)80013-2.
[163] M. Lorentzon, S.R. Cummings, Osteoporosis: the evolution of a diagnosis, J Intern Med 277(6) (2015) 650-61 10.1111/joim.12369.
[164] J.A. Kanis, Assessment of fracture risk and its application to screening for postmenopausal osteoporosis: synopsis of a WHO report. WHO Study Group, Osteoporos Int 4(6) (1994) 368-81 10.1007/bf01622200.
[165] M. Chen, H. Yuan, Assessment of porosity index of the femoral neck and tibia by 3D ultra-short echo-time MRI, J Magn Reson Imaging 47(3) (2018) 820-828 10.1002/jmri.25782.
[166] S. Rokidi, E.P. Paschalis, K. Klaushofer, S. Vennin, A. Desyatova, J.A. Turner, P. Watson, J. Lappe, M.P. Akhter, R.R. Recker, Organic matrix quality discriminates between age- and BMD-matched fracturing versus non-fracturing post-menopausal women: A pilot study, Bone 127 (2019) 207-214 10.1016/j.bone.2019.06.017.
[167] S. Vennin, A. Desyatova, J.A. Turner, P.A. Watson, J.M. Lappe, R.R. Recker, M.P. Akhter, Intrinsic material property differences in bone tissue from patients suffering low-trauma osteoporotic fractures, compared to matched non-fracturing women, Bone 97 (2017) 233-242 10.1016/j.bone.2017.01.031.
[168] T. Sukenari, M. Horii, K. Ikoma, M. Kido, S. Hayashi, Y. Hara, T. Yamasaki, K. Matsuda, M. Kawata, T. Kubo, Cortical bone water changes in ovariectomized rats during the early postoperative period: Objective evaluation using sweep imaging with Fourier transform, J Magn Reson Imaging 42(1) (2015) 128-35 10.1002/jmri.24765.
[169] R.K. Surowiec, S. Ram, D. Idiyatullin, R. Goulet, S.H. Schlecht, C.J. Galban, K.M. Kozloff, In vivo quantitative imaging biomarkers of bone quality and mineral density using multi-band-SWIFT magnetic resonance imaging, Bone 143 (2021) 115615 10.1016/j.bone.2020.115615.
[170] T.L. Nickolas, M.B. Leonard, E. Shane, Chronic kidney disease and bone fracture: a growing concern, Kidney Int 74(6) (2008) 721-31 10.1038/ki.2008.264.
[171] J. Mitome, H. Yamamoto, M. Saito, K. Yokoyama, K. Marumo, T. Hosoya, Nonenzymatic cross-linking pentosidine increase in bone collagen and are associated with disorders of bone mineralization in dialysis patients, Calcif Tissue Int 88(6) (2011) 521-9 10.1007/s00223-011-9488-y.
[172] Y. Iwasaki, J.J. Kazama, H. Yamato, A. Matsugaki, T. Nakano, M. Fukagawa, Altered material properties are responsible for bone fragility in rats with chronic kidney injury, Bone 81 (2015) 247-254 10.1016/j.bone.2015.07.015.
[173] C.L. Newman, S.M. Moe, N.X. Chen, M.A. Hammond, J.M. Wallace, J.S. Nyman, M.R. Allen, Cortical bone mechanical properties are altered in an animal model of progressive chronic kidney disease, PLoS One 9(6) (2014) e99262 10.1371/journal.pone.0099262.
[174] E.M.B. McNerny, D.T. Buening, M.W. Aref, N.X. Chen, S.M. Moe, M.R. Allen, Time course of rapid bone loss and cortical porosity formation observed by longitudinal μCT in a rat model of CKD, Bone 125 (2019) 16-24 10.1016/j.bone.2019.05.002.
[175] P. Vestergaard, Discrepancies in bone mineral density and fracture risk in patients with type 1 and type 2 diabetes--a meta-analysis, Osteoporos Int 18(4) (2007) 427-44 10.1007/s00198-006-0253-4.

[176] J.N. Farr, S. Khosla, Determinants of bone strength and quality in diabetes mellitus in humans, Bone 82 (2016) 28-34 10.1016/j.bone.2015.07.027.
[177] S. Rokidi, V.F.C. Andrade, V. Borba, E. Shane, A. Cohen, J. Zwerina, E.P. Paschalis, C.A. Moreira, Bone tissue material composition is compromised in premenopausal women with Type 2 diabetes, Bone 141 (2020) 115634 10.1016/j.bone.2020.115634.
[178] M. Minami, K. Ikoma, M. Horii, T. Sukenari, O. Onishi, H. Fujiwara, H. Ogi, K. Itoh, T. Kubo, Usefulness of Sweep Imaging With Fourier Transform for Evaluation of Cortical Bone in Diabetic Rats, J Magn Reson Imaging 48(2) (2018) 389-397 10.1002/jmri.25955.
[179] F.S. Van Dijk, D.O. Sillence, Osteogenesis imperfecta: clinical diagnosis, nomenclature and severity assessment, Am J Med Genet A 164a(6) (2014) 1470-81 10.1002/ajmg.a.36545.
[180] J.C. Marini, A. Forlino, H.P. Bächinger, N.J. Bishop, P.H. Byers, A. Paepe, F. Fassier, N. Fratzl-Zelman, K.M. Kozloff, D. Krakow, K. Montpetit, O. Semler, Osteogenesis imperfecta, Nat Rev Dis Primers 3 (2017) 17052 10.1038/nrdp.2017.52.
[181] R.K. Surowiec, L.F. Battle, F.S. Ward, S.H. Schlecht, B.M. Khoury, C. Robbins, E.M. Wojtys, M.S. Caird, K.M. Kozloff, A xenograft model to evaluate the bone forming effects of sclerostin antibody in human bone derived from pediatric osteogenesis imperfecta patients, Bone 130 (2020) 115118 10.1016/j.bone.2019.115118.
[182] N.P. Camacho, P. Carroll, C.L. Raggio, Fourier transform infrared imaging spectroscopy (FT-IRIS) of mineralization in bisphosphonate-treated oim/oim mice, Calcif Tissue Int 72(5) (2003) 604-9 10.1007/s00223-002-1038-1.
[183] R.Z. Kramer, M.G. Venugopal, J. Bella, P. Mayville, B. Brodsky, H.M. Berman, Staggered molecular packing in crystals of a collagen-like peptide with a single charged pair, J Mol Biol 301(5) (2000) 1191-205 10.1006/jmbi.2000.4017.
[184] R. Ailavajhala, W. Querido, C.S. Rajapakse, N. Pleshko, Near infrared spectroscopic assessment of loosely and tightly bound cortical bone water, Analyst 145(10) (2020) 3713-3724 10.1039/c9an02491c.
[185] S.D. Mooney, T.E. Klein, Structural models of osteogenesis imperfecta-associated variants in the COL1A1 gene, Mol Cell Proteomics 1(11) (2002) 868-75 10.1074/mcp.m200064-mcp200.
[186] N. Shanas, W. Querido, J. Oswald, K. Jepsen, E. Carter, C. Raggio, N. Pleshko, EXPRESS: Infrared Spectroscopy-Determined Bone Compositional Changes Associated with Anti-Resorptive Treatment of the Oim/Oim Mouse Model of Osteogenesis Imperfecta, Appl Spectrosc 10.1177/00037028211055477 (2021) 37028211055477 10.1177/00037028211055477.
[187] O.G. Andriotis, S.W. Chang, M. Vanleene, P.H. Howarth, D.E. Davies, S.J. Shefelbine, M.J. Buehler, P.J. Thurner, Structure–mechanics relationships of collagen fibrils in the osteogenesis imperfecta mouse model, Journal of The Royal Society Interface 12(111) (2015) 20150701 doi:10.1098/rsif.2015.0701.
[188] E. Seeman, Overview of bone microstructure, and treatment of bone fragility in chronic kidney disease, Nephrology (Carlton) 22 Suppl 2 (2017) 34-35 10.1111/nep.13024.
[189] S. Gourion-Arsiquaud, M.R. Allen, D.B. Burr, D. Vashishth, S.Y. Tang, A.L. Boskey, Bisphosphonate treatment modifies canine bone mineral and matrix properties and their heterogeneity, Bone 46(3) (2010) 666-72 10.1016/j.bone.2009.11.011.
[190] M.R. Allen, E. Gineyts, D.J. Leeming, D.B. Burr, P.D. Delmas, Bisphosphonates alter trabecular bone collagen cross-linking and isomerization in beagle dog vertebra, Osteoporos Int 19(3) (2008) 329-37 10.1007/s00198-007-0533-7.
[191] M.R. Allen, D.B. Burr, Bisphosphonate effects on bone turnover, microdamage, and mechanical properties: what we think we know and what we know that we don't know, Bone 49(1) (2011) 56-65 10.1016/j.bone.2010.10.159.
[192] C. Acevedo, H. Bale, B. Gludovatz, A. Wat, S.Y. Tang, M. Wang, B. Busse, E.A. Zimmermann, E. Schaible, M.R. Allen, D.B. Burr, R.O. Ritchie, Alendronate treatment alters bone tissues at multiple structural levels in healthy canine cortical bone, Bone 81 (2015) 352-363 10.1016/j.bone.2015.08.002.
[193] J.R. Rey, E.V. Cervino, M.L. Rentero, E.C. Crespo, A.O. Alvaro, M. Casillas, Raloxifene: mechanism of action, effects on bone tissue, and applicability in clinical traumatology practice, Open Orthop J 3 (2009) 14-21 10.2174/1874325000903010014.
[194] B. Ettinger, D.M. Black, B.H. Mitlak, R.K. Knickerbocker, T. Nickelsen, H.K. Genant, C. Christiansen, P.D. Delmas, J.R. Zanchetta, J. Stakkestad, C.C. Glüer, K. Krueger, F.J. Cohen, S. Eckert, K.E. Ensrud, L.V. Avioli, P. Lips, S.R. Cummings, Reduction of vertebral fracture risk in postmenopausal women with osteoporosis treated with raloxifene: results from a 3-year randomized clinical trial. Multiple Outcomes of Raloxifene Evaluation (MORE) Investigators, Jama 282(7) (1999) 637-45 10.1001/jama.282.7.637.
[195] B.L. Riggs, L.J. Melton, 3rd, Bone turnover matters: the raloxifene treatment paradox of dramatic decreases in vertebral fractures without commensurate increases in bone density, J Bone Miner Res 17(1) (2002) 11-4 10.1359/jbmr.2002.17.1.11.
[196] S. Sarkar, B.H. Mitlak, M. Wong, J.L. Stock, D.M. Black, K.D. Harper, Relationships between bone mineral density and incident vertebral fracture risk with raloxifene therapy, J Bone Miner Res 17(1) (2002) 1-10 10.1359/jbmr.2002.17.1.1.
[197] D.E. Jacobsen, M.M. Samson, M.H. Emmelot-Vonk, H.J. Verhaar, Raloxifene and body composition and muscle strength in postmenopausal women: a randomized, double-blind, placebo-controlled trial, Eur J Endocrinol 162(2) (2010) 371-6 10.1530/eje-09-0619.

[198] N. Bivi, H. Hu, B. Chavali, M.J. Chalmers, C.T. Reutter, G.L. Durst, A. Riley, M. Sato, M.R. Allen, D.B. Burr, J.A. Dodge, Structural features underlying raloxifene's biophysical interaction with bone matrix, Bioorg Med Chem 24(4) (2016) 759-67 10.1016/j.bmc.2015.12.045.
[199] M.R. Allen, P.R. Territo, C. Lin, S. Persohn, L. Jiang, A.A. Riley, B.P. McCarthy, C.L. Newman, D.B. Burr, G.D. Hutchins, In Vivo UTE-MRI Reveals Positive Effects of Raloxifene on Skeletal-Bound Water in Skeletally Mature Beagle Dogs, J Bone Miner Res 30(8) (2015b) 1441-4 10.1002/jbmr.2470.
[200] M.R. Allen, E. McNerny, M. Aref, J.M. Organ, C.L. Newman, B. McGowan, T. Jang, D.B. Burr, D.M. Brown, M. Hammond, P.R. Territo, C. Lin, S. Persohn, L. Jiang, A.A. Riley, B.P. McCarthy, G.D. Hutchins, J.M. Wallace, Effects of combination treatment with alendronate and raloxifene on skeletal properties in a beagle dog model, PLoS One 12(8) (2017) e0181750 10.1371/journal.pone.0181750.
[201] M.R. Eby, D.M. Cristino, M. Counihan, K.M. Masada, J. Ahn, M.W. Hast, Immersion in Raloxifene does not significantly improve bone toughness or screw pull-out strength in multiple in vitro models, BMC Musculoskelet Disord 22(1) (2021) 468 10.1186/s12891-021-04342-1.
[202] C.A. Tastad, R. Kohler, J.M. Wallace, Limited impacts of thermoneutral housing on bone morphology and mechanical properties in growing female mice exposed to external loading and raloxifene treatment, Bone 146 (2021) 115889 https://doi.org/10.1016/j.bone.2021.115889.
[203] K.M. Powell, C. Skaggs, A. Pulliam, A. Berman, M.R. Allen, J.M. Wallace, Zoledronate and Raloxifene combination therapy enhances material and mechanical properties of diseased mouse bone, Bone 127 (2019) 199-206 10.1016/j.bone.2019.06.018.
[204] G. Wang, W. Xu, J. Zhang, T. Tang, J. Chen, C. Fan, Induction of Bone Remodeling by Raloxifene-Doped Iron Oxide Functionalized with Hydroxyapatite to Accelerate Fracture Healing, J Biomed Nanotechnol 17(5) (2021b) 932-941 10.1166/jbn.2021.3068.
[205] K.M. Powell, A.P. Brown, C.G. Skaggs, A.N. Pulliam, A.G. Berman, P. Deosthale, L.I. Plotkin, M.R. Allen, D.R. Williams, J.M. Wallace, 6'-Methoxy Raloxifene-analog enhances mouse bone properties with reduced estrogen receptor binding, Bone reports 12 (2020) 100246-100246 10.1016/j.bonr.2020.100246.
[206] G. Kerch, Role of Changes in State of Bound Water and Tissue Stiffness in Development of Age-Related Diseases, Polymers (Basel) 12(6) (2020) 10.3390/polym12061362.

Highlights

- Bone water can greatly influence mechanical properties and tissue quality.
- Bone water is found as free/pore, loosely bound, tightly bound, and structural water.
- Bone hydration can dynamically change due to healthy aging, disease, and treatment.
- Imaging and spectroscopic advances have made the study of bone water possible.
- Therapeutically targeting bone water may be efficacious in improving mechanical properties.

Figure 1

Click here to access/download;Figure(s);Figure 1_Water across 4 distinct compartments.png

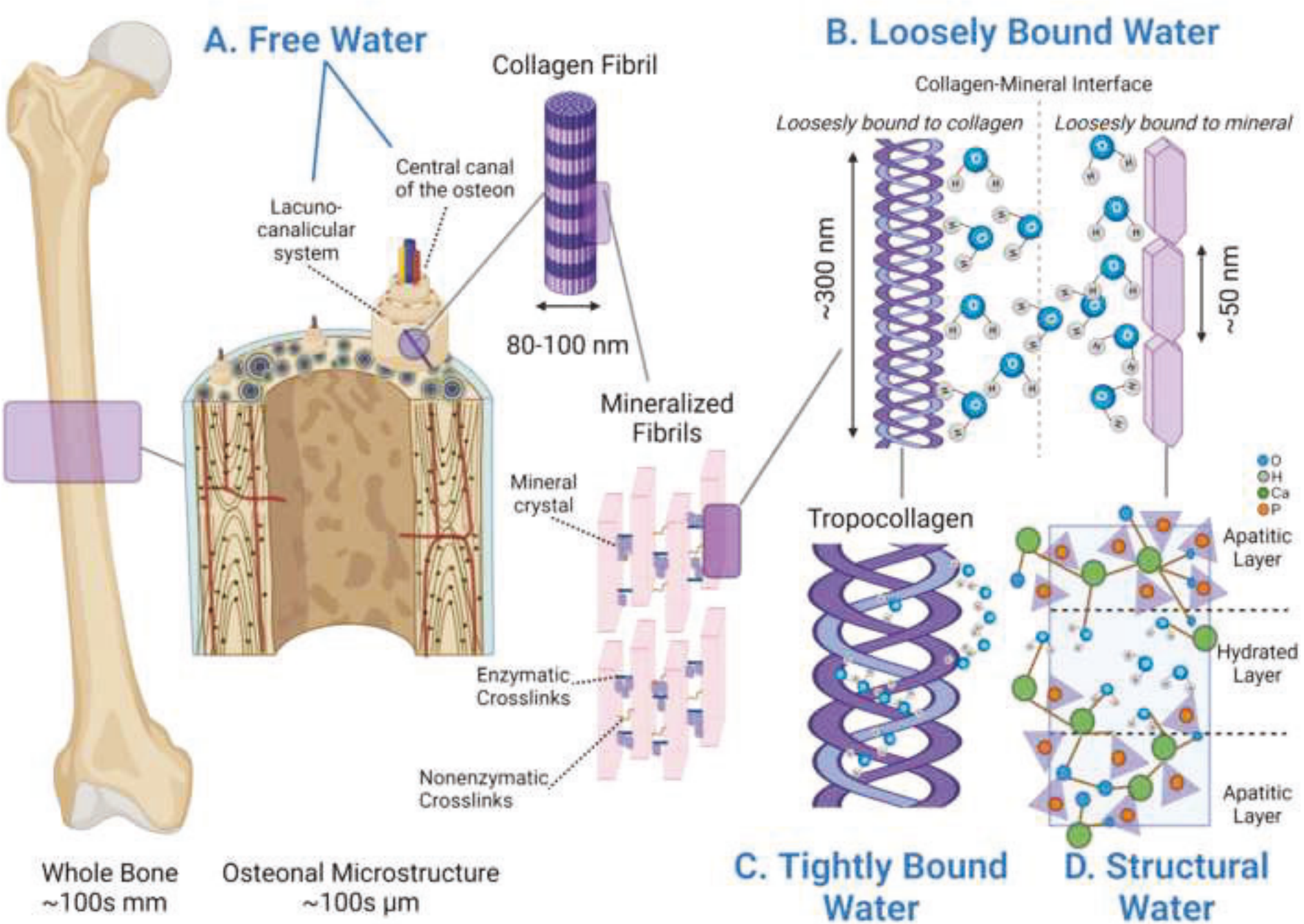

Figure 2

Click here to access/download;Figure(s);Figure 2_Force_Disp Stress_Strain w_ water compartments.png

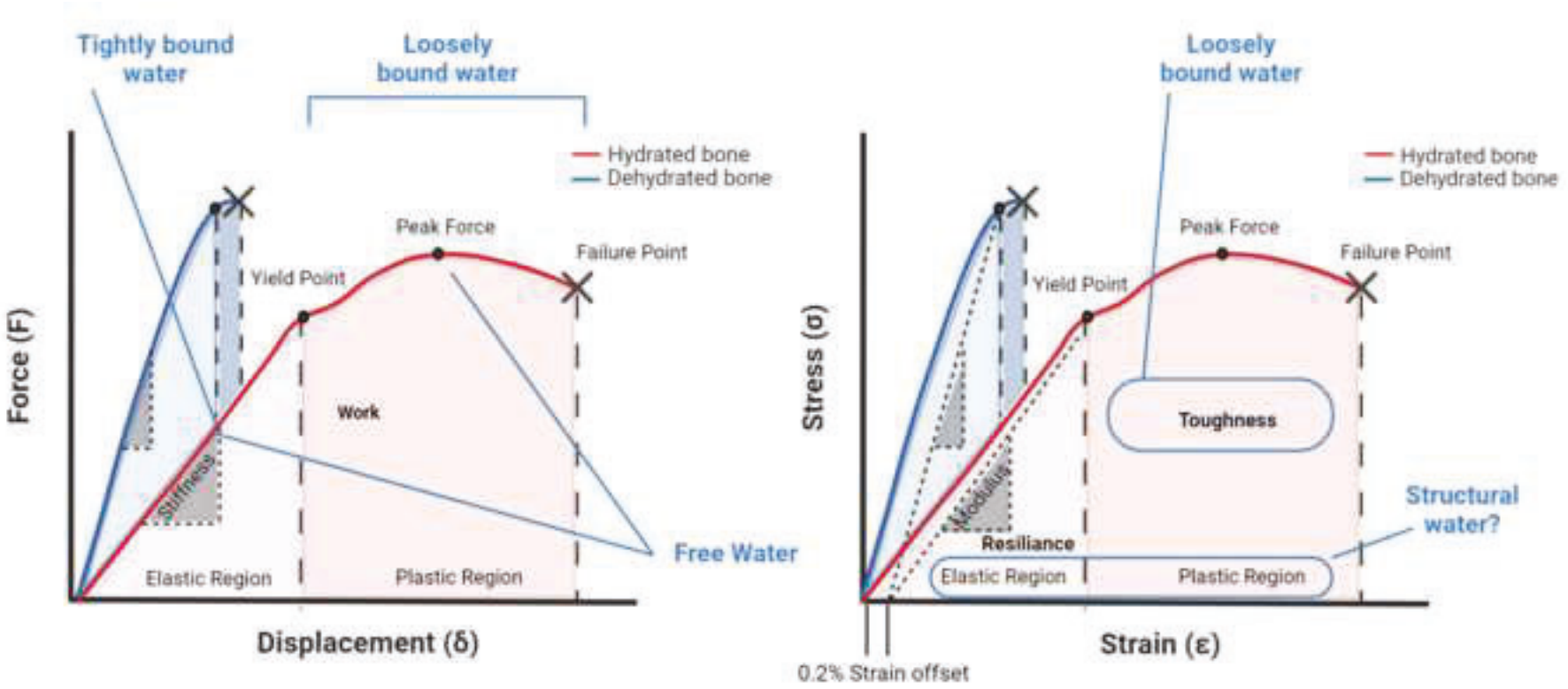

Figure 3

Click here to access/download;Figure(s);Figure 3_bone reports_hydration rev_1000dpi.tif

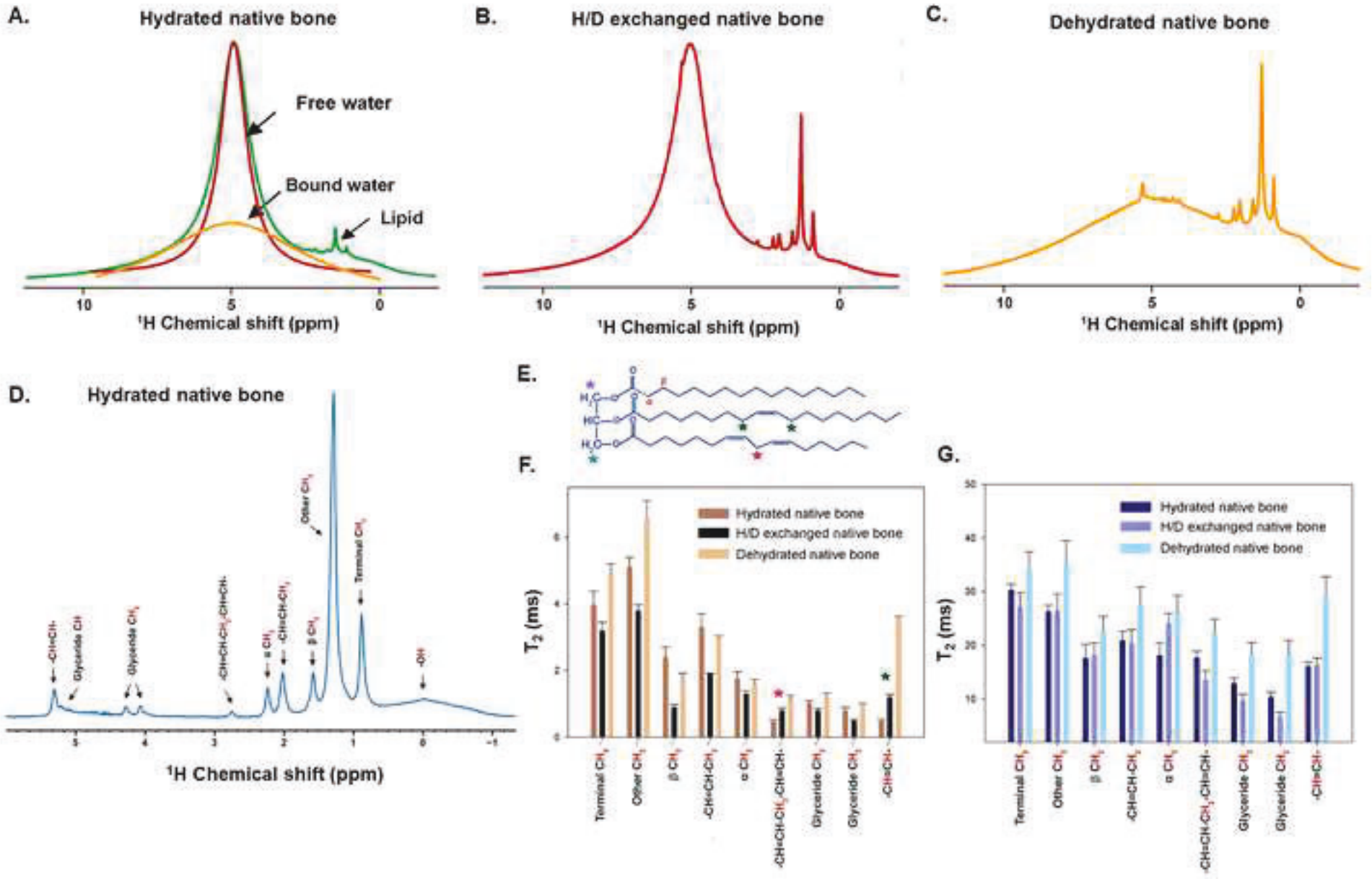

Figure 4

Click here to access/download;Figure(s);Figure 4_bone reports_hydration rev_1000dpi.tif

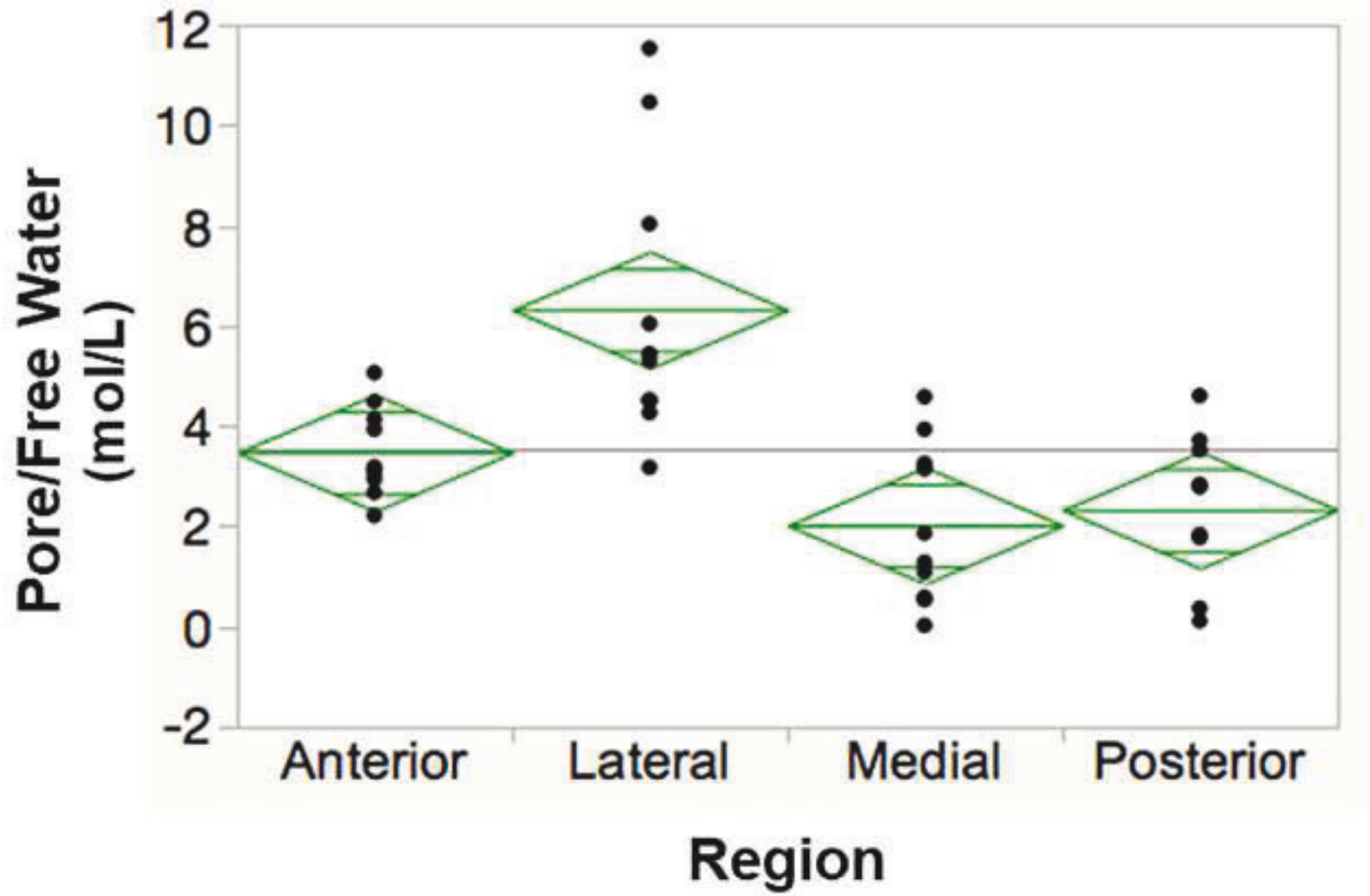

Figure 5

Click here to access/download;Figure(s);Figure 5_bone reports_hydration rev_1000dpi.tif

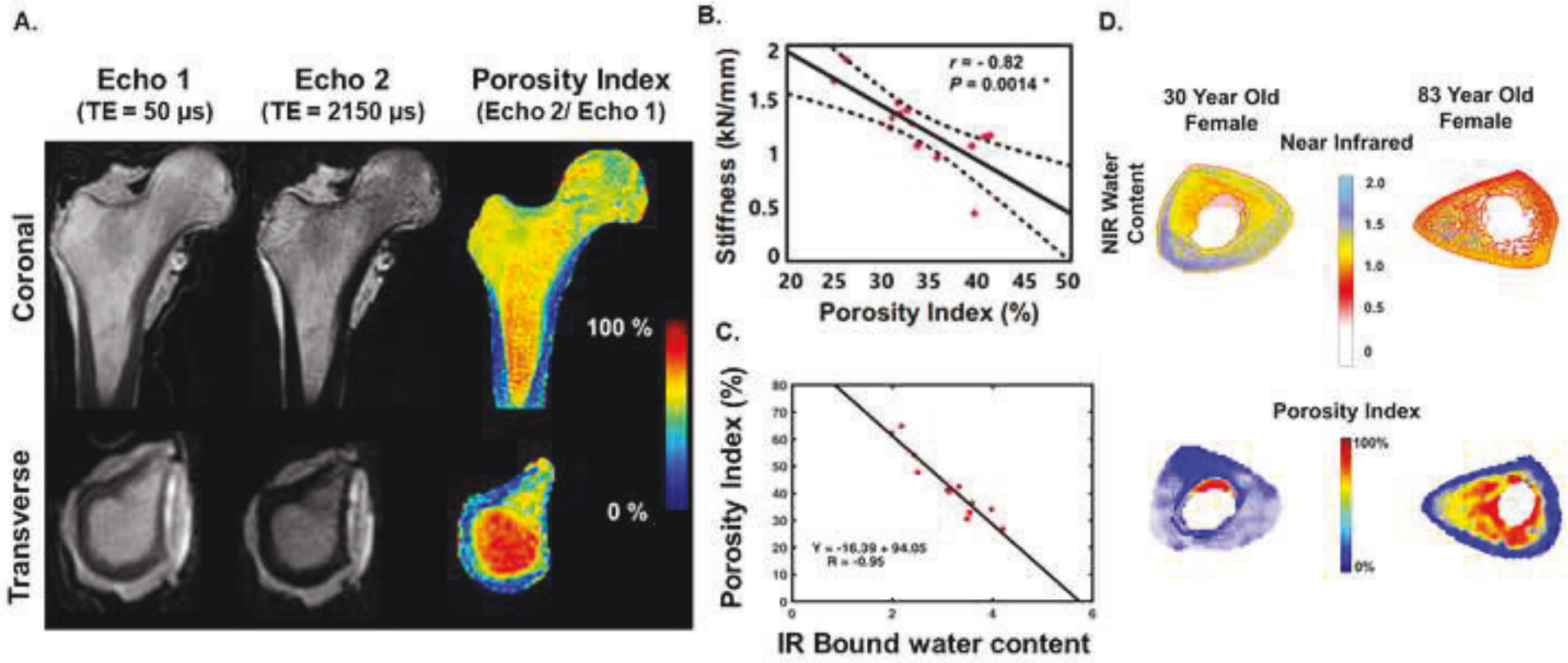

Figure 6

Click here to access/download;Figure(s);Figure 6_bone reports_hydration rev_1000dpi.tif

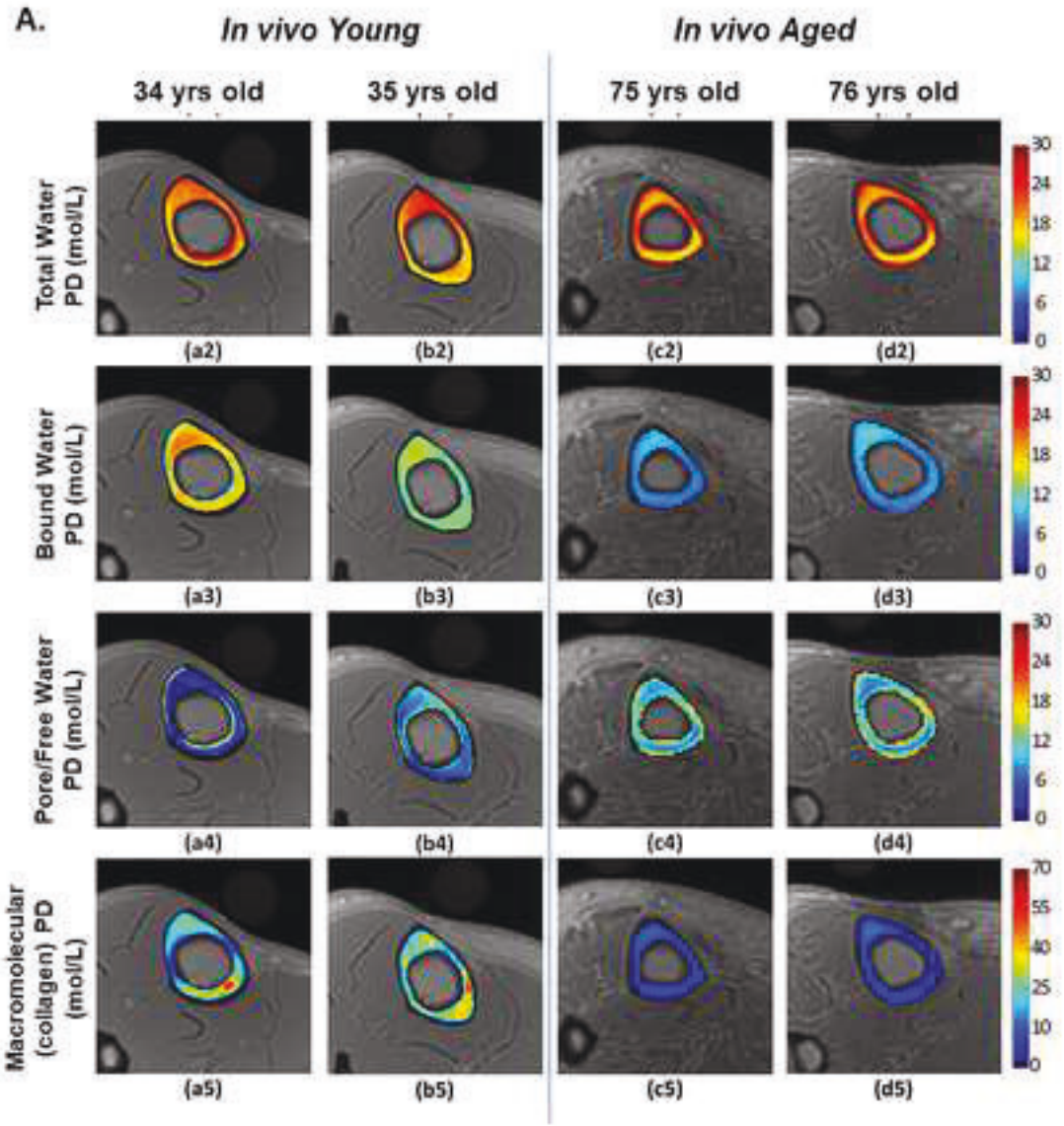

B.

	TWPD (mol/L)	BWPD (mol/L)	PWPD (mol/L)	MMPD (mol/L)
In vivo Young	29.3 ± 6.3	14.8 ± 2.2	14.8 ± 5.3	45.8 ± 12.4
In vivo Aged	36.4 ± 8.3	13.0 ± 1.7	23.4 ± 8.7	29.8 ± 14.8

TWPD, BWPD, PWPD, and MMPD: total water, bound water, pore/free water, and macromolecular proton density, respectively

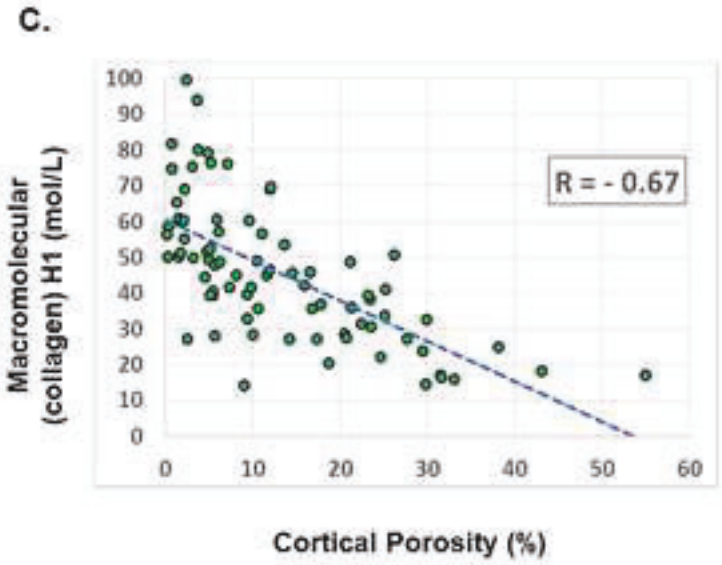

Figure 7

Click here to access/download;Figure(s);Figure 7_bone reports_hydration rev_1000dpi.tif

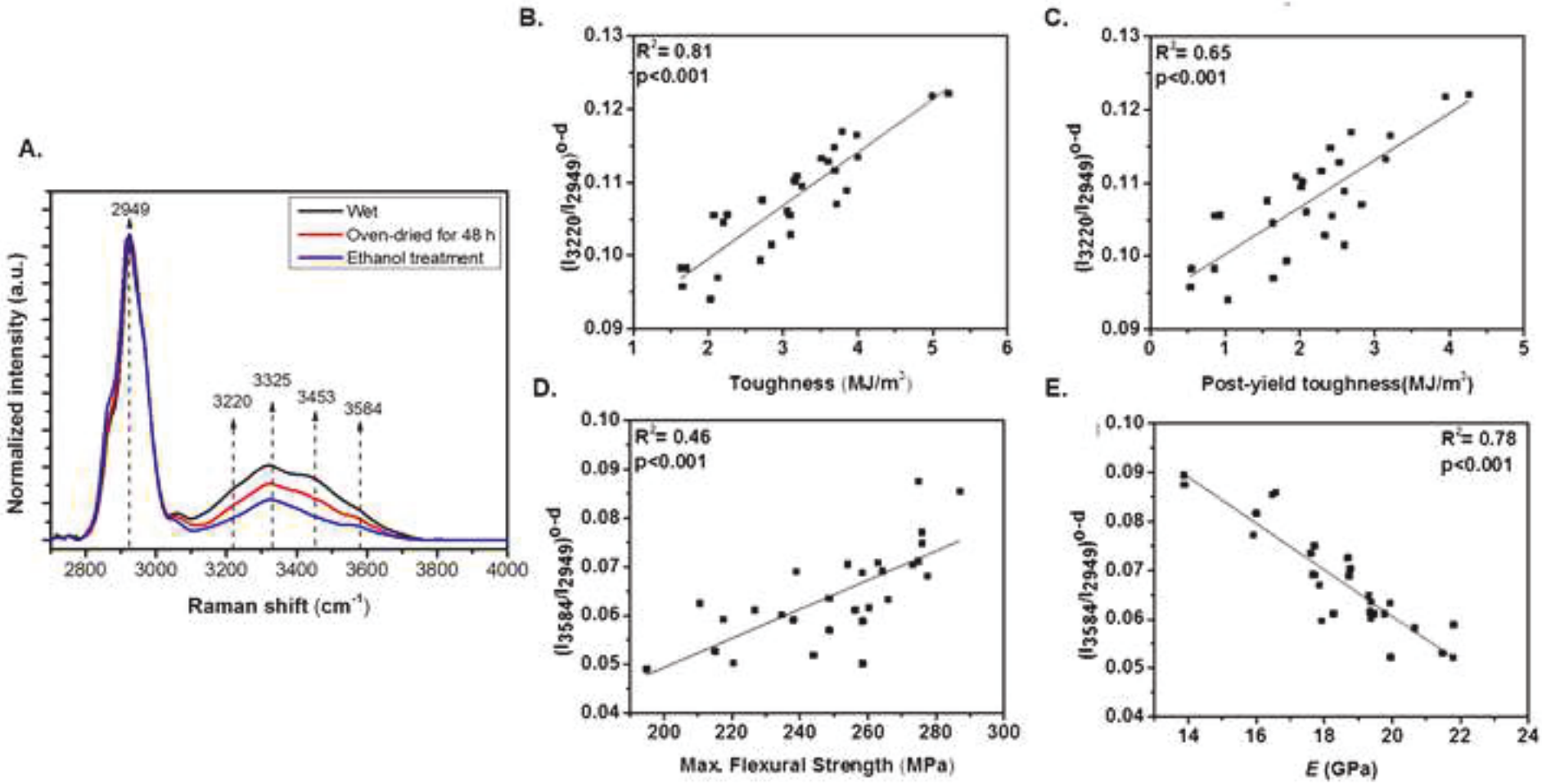

Figure 8

Click here to access/download;Figure(s);Figure 8_bone reports_hydration rev_1000dpi.tif

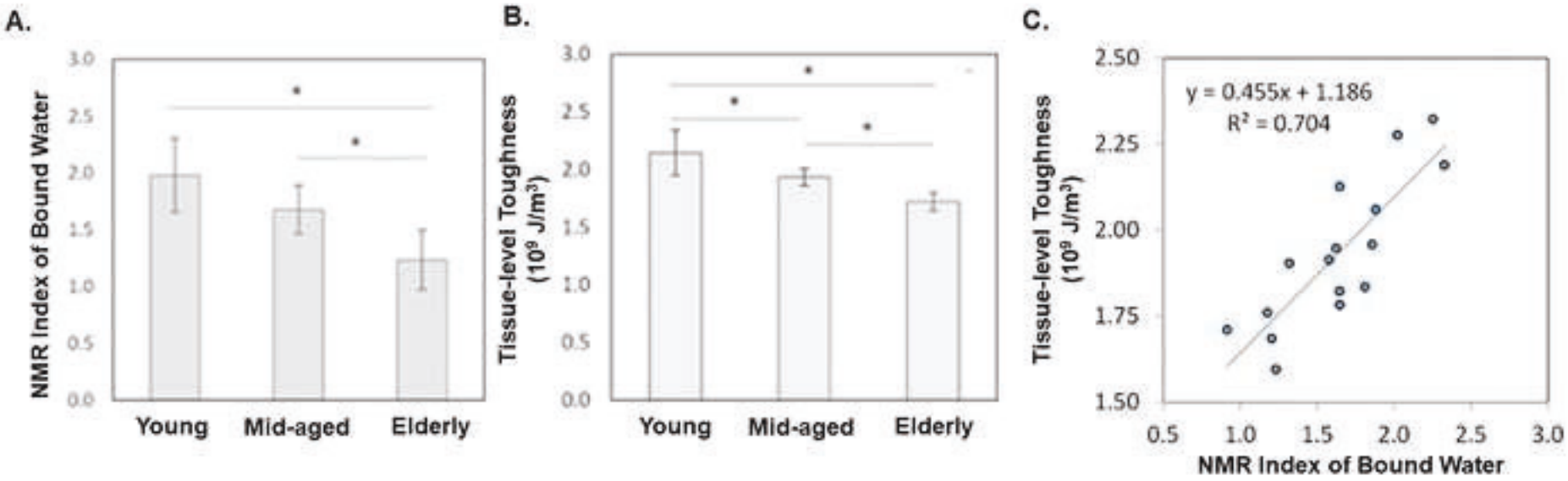

Figure 9

Click here to access/download;Figure(s);Figure 9_bone reports_hydration rev_1000dpi.tif

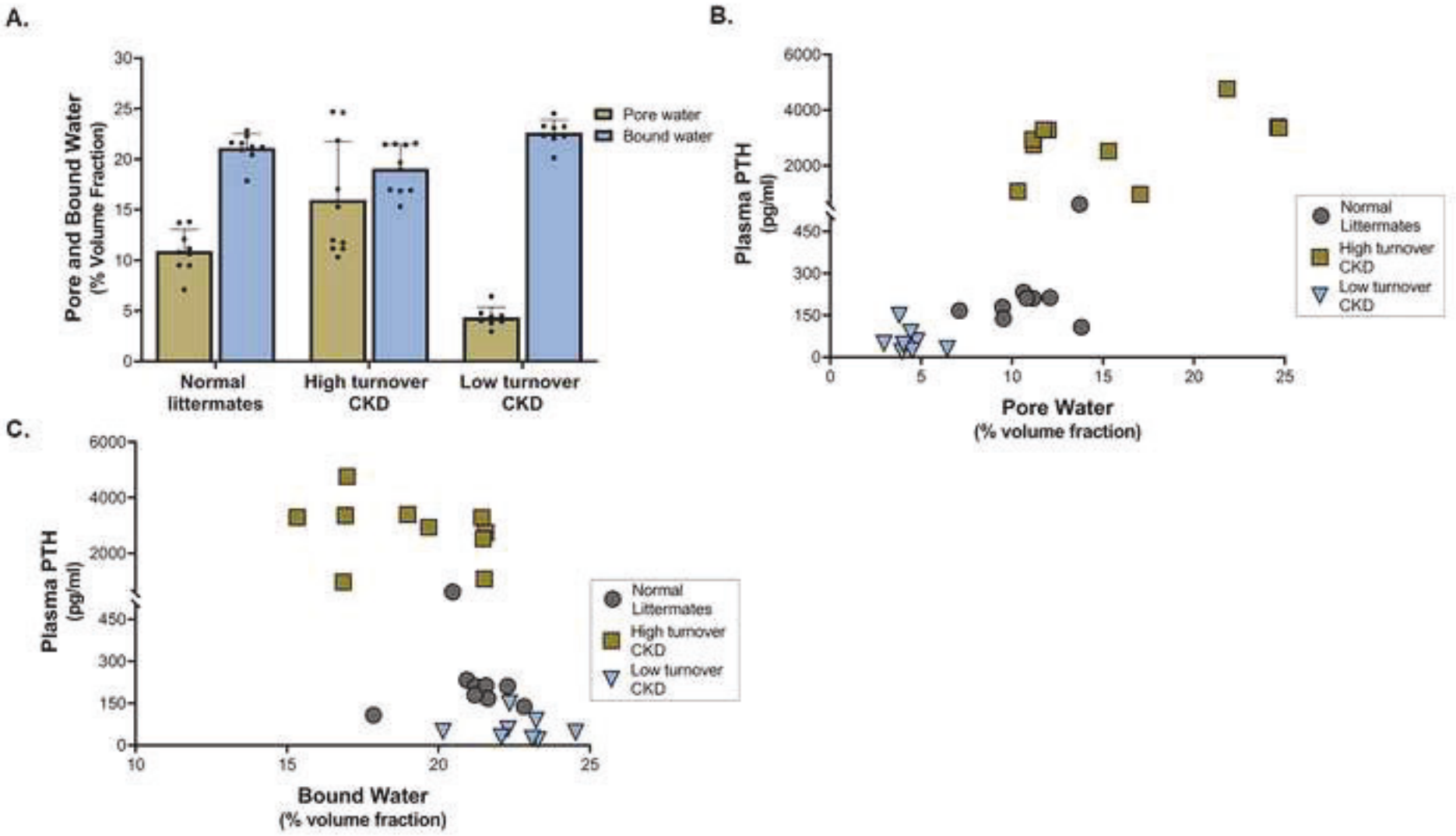

Figure 10

Click here to access/download;Figure(s);Figure 10_bone reports_hydration rev_1000dpi.tif

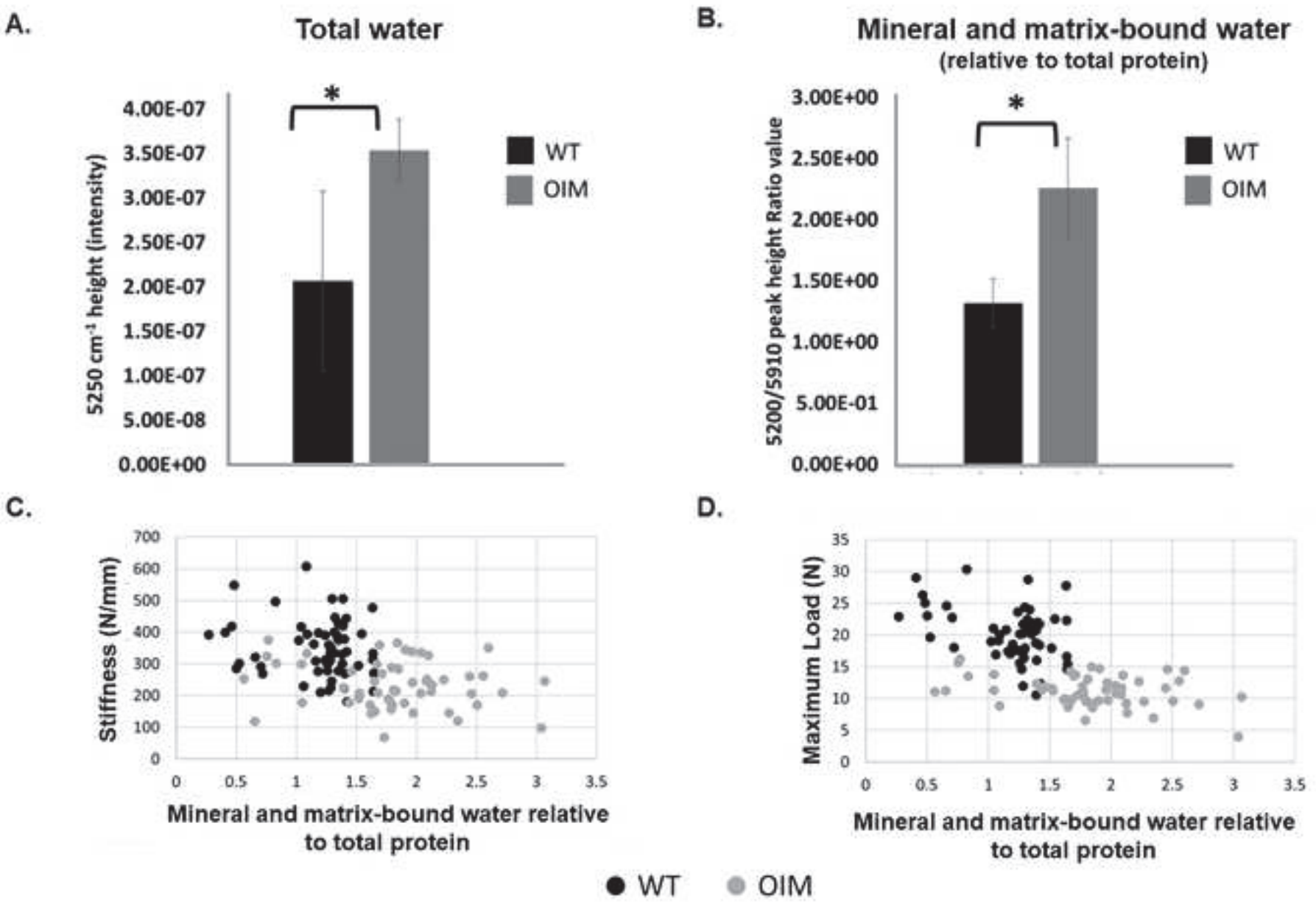

Figure 11

Click here to access/download;Figure(s);Figure 11_bone reports_hydration rev_1000dpi.tif

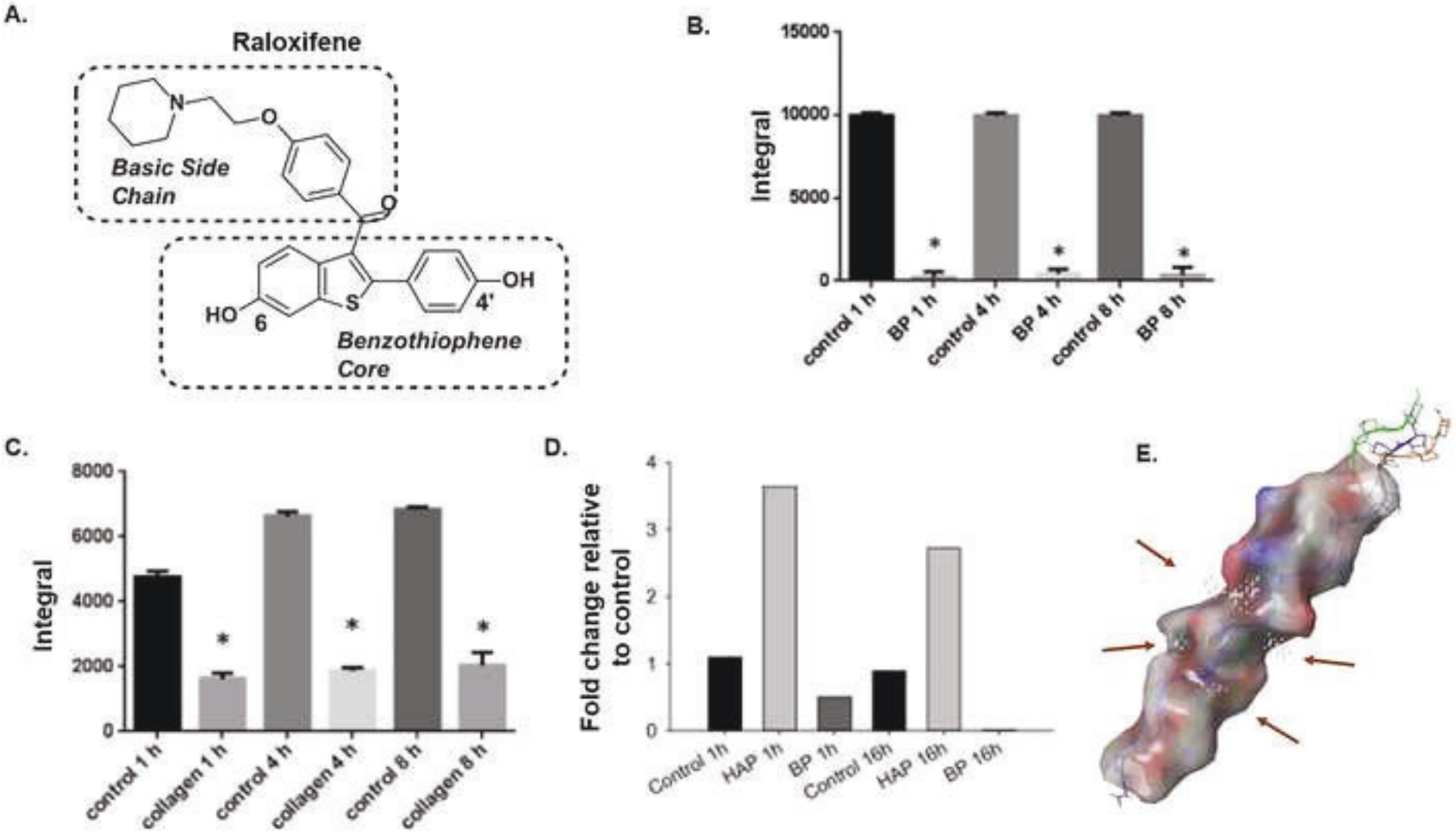

Figure 12

Click here to access/download;Figure(s);Figure 12_bone reports_hydration rev_1000dpi.tif

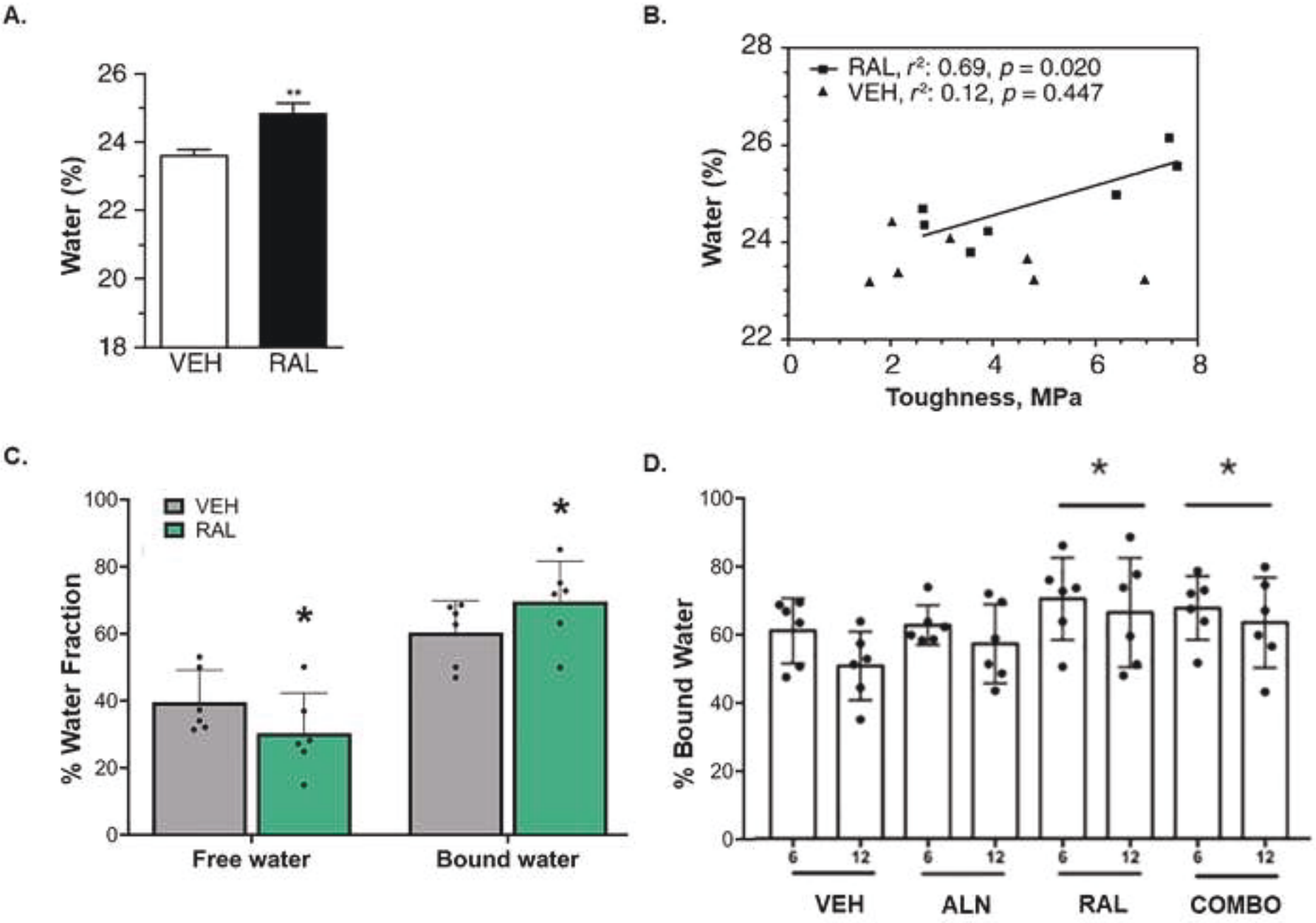

CRediT Author Statement

Rachel K. Surowiec: Conceptualization, Writing-Original Draft. **Matthew R. Allen**: Conceptualization, Writing-Review & Editing. **Joseph M. Wallace**: Conceptualization, Writing-Review & Editing.